


2016

Ability of an acoustic Doppler current profiler to measure turbulence and mixing

Lauren Elise Schwab
Iowa State University

Follow this and additional works at: <https://lib.dr.iastate.edu/etd>

 Part of the [Civil Engineering Commons](#), and the [Environmental Engineering Commons](#)

Recommended Citation

Schwab, Lauren Elise, "Ability of an acoustic Doppler current profiler to measure turbulence and mixing" (2016). *Graduate Theses and Dissertations*. 15058.

<https://lib.dr.iastate.edu/etd/15058>

This Thesis is brought to you for free and open access by the Iowa State University Capstones, Theses and Dissertations at Iowa State University Digital Repository. It has been accepted for inclusion in Graduate Theses and Dissertations by an authorized administrator of Iowa State University Digital Repository. For more information, please contact digirep@iastate.edu.

Ability of an acoustic Doppler current profiler to measure turbulence and mixing

by

Lauren Elise Schwab

A thesis submitted to the graduate faculty
in partial fulfillment of the requirements for the degree of

MASTER OF SCIENCE

Major: Civil Engineering (Environmental Engineering)

Program of Study Committee:
Chris Rehmman, Major Professor
Kristie Franz
Roy Gu

Iowa State University

Ames, Iowa

2016

Copyright © Lauren Elise Schwab, 2016. All rights reserved.

To Larry Hansen.

Thank you for always encouraging me to be better at everything I did.

TABLE OF CONTENTS

LIST OF TABLES	v
LIST OF FIGURES	vi
ACKNOWLEDGMENTS	viii
ABSTRACT	ix
NOTATION LIST	x
CHAPTER 1: INTRODUCTION	1
Significance	1
Objectives	2
Hypothesis	2
Outline	3
CHAPTER 2: BACKGROUND	4
Importance	4
Methods for Measuring and Estimating the Dispersion and Mixing Coefficients	4
Measuring the Dispersion Coefficient	5
Measuring the Transverse Mixing Coefficient	8
Empirical Estimates for Mixing and their Shortcomings	11
ADCP Method of Measuring the Dispersion Coefficient	13
Brief Introduction to Shear Dispersion Theory	13
Examples of ADCPs in Measuring the Dispersion Coefficient	15
The Mixing Coefficient as a Limitation	17
The Ability of the ADCP to Measure Mean Velocity and Turbulence	18
Importance of Statistical Homogeneity	20
Summary	20
CHAPTER 3: METHODS	23
Experimental Facility	23
Equipment	25
RD Instruments StreamPro Acoustic Doppler Current Profiler	26
Nortek Acoustic Doppler Velocimeter	28
Experiment Design	30
Processing	32

CHAPTER 4: RESULTS AND DISCUSSION.....	37
Introduction.....	37
Evaluation of Sampling Conditions.....	37
Comparison of Mean Velocity.....	41
Comparison of Reynolds Stresses and Turbulent Kinetic Energy.....	46
Transverse Mixing Coefficient Estimates.....	54
CHAPTER 5: CONCLUSIONS.....	57
Summary.....	57
Recommendations and Future Work.....	60
APPENDIX A: IMPORTANCE OF VERTICAL VARIATIONS OF VELOCITY FOR SHEAR DISPERSION IN RIVERS.....	61
APPENDIX B: MATLAB SCRIPTS USED IN READING AND PROCESSING ADCP AND ADV DATA.....	84
ADCP Utilities.....	84
ADCP_read_2.....	84
ADCP_process_f.....	86
ADV Utilities.....	89
ADV_read_condensed.....	89
ADV_process_f.....	91
REFERENCES.....	92

LIST OF TABLES

Table 1 – Selection of empirical equations for estimating the dispersion coefficient	8
Table 2 - Selection of empirical estimates for the transverse mixing coefficient	11
Table 3 - Processing combinations and error bounds estimated from Figure 4 of Shen et al. (2010).....	16
Table 4 - WinRiver II measurement wizard settings	28
Table 5 - Vectrino+ software settings.....	30
Table 6 - WinRiverII output ASCII template	32

LIST OF FIGURES

Figure 1 - Range of transverse mixing coefficient for five different locations. The dataset for each location was processed using four standard empirical equations. Data from Nordin and Sabol (1974), McQuivey and Keefer (1974), Rutherford (1994), and Seo and Cheong (1998)	12
Figure 2 - Plan view of the flume.....	24
Figure 3 - Pump & flume system schematic	25
Figure 4 - RDInstruments StreamPro ADCP Schematic	26
Figure 5 – StreamPro transducer mounting position (top); Instrument and beam orientation (bottom).....	27
Figure 6 - Nortek ADV schematic (left); ADV mounting apparatus (right)	29
Figure 7 - Projection of ADCP beam velocity onto each axis for beam 2	33
Figure 8 – Cumulative average of streamwise velocity at 9cm above the bed.	38
Figure 9 – Averaged frequency spectrum calculated for data collected at $y = 0$ and $z = 5\text{cm}$	39
Figure 10 – Averaged frequency spectrum calculated for data collected 5cm from the bed in the center of the channel.....	40
Figure 11 - ADCP intensity profiles for $H/B = 0.47$ (left) and $H/B = 0.53$ (right).....	41
Figure 12 – Streamwise velocity profiles obtained by ADV and ADCP for $H/B = 0.47$ (left) and $H/B = 0.53$ (right).....	43
Figure 13 – Vertical profiles of transverse velocity obtained by ADV and ADCP for $H/B = 0.47$ (left) and $H/B = 0.53$ (right).....	44
Figure 14 - Vertical profiles for vertical velocity obtained by ADV and ADCP for $H/B = 0.47$ (left) and $H/B = 0.53$ (right)	45
Figure 15 - Absolute difference in beam velocity pairs for $H/B = 0.47$ (left) and $H/B = 0.53$ (right).....	46
Figure 16 – ADV and ADCP measured Reynolds shear stress profiles for $H/B = 0.47$: - $\langle u'v' \rangle$ (top left); - $\langle v'w' \rangle$ (top center); - $\langle u'w' \rangle$ (top right); and $H/B = 0.53$: - $\langle u'v' \rangle$ (bottom left); - $\langle v'w' \rangle$ (bottom center); - $\langle u'w' \rangle$ (bottom right).....	48
Figure 17 - ADV and ADCP measured Reynolds normal stress profiles for $H/B = 0.47$: - $\langle u'^2 \rangle$ (top left); - $\langle v'^2 \rangle$ (top center); - $\langle w'^2 \rangle$ (top right); and $H/B = 0.53$: - $\langle u'^2 \rangle$ (bottom left); - $\langle v'^2 \rangle$ (bottom center); - $\langle w'^2 \rangle$ (bottom right).....	50
Figure 18 – Percent error in Reynolds shear stresses for $H/B = 0.47$ (top left) and $H/B = 0.53$ (top right); Percent error in Reynolds normal stresses for $H/B = 0.47$ (bottom left) and $H/B = 0.53$ (bottom right).....	51
Figure 19 - ADV and ADCP measured Reynolds shear stress profiles calculated two ways for $H/B = 0.47$: - $\langle u'v' \rangle$ (top left); - $\langle v'w' \rangle$ (top center); - $\langle u'w' \rangle$ (top right); and $H/B = 0.53$: - $\langle u'v' \rangle$ (bottom left); - $\langle v'w' \rangle$ (bottom center); - $\langle u'w' \rangle$ (bottom right).....	52

Figure 20 - ADV and ADCP measured Reynolds normal stress profiles calculated two ways for $H/B = 0.47$: $-\langle u'^2 \rangle$ (top left); $-\langle v'^2 \rangle$ (top center); $-\langle w'^2 \rangle$ (top right); and $H/B = 0.53$: $-\langle u'^2 \rangle$ (bottom left); $-\langle v'^2 \rangle$ (bottom center); $-\langle w'^2 \rangle$ (bottom right).	53
Figure 21 - TKE profiles for H/B of 2.1 (left) and 0.53 (right).	54
Figure 22 - Transverse mixing coefficient estimates for flume flow for $H/B = 0.47$ (left) and $H/B = 0.53$ (right)	55

ACKNOWLEDGMENTS

Many individuals have been a part of my graduate adventure. First, this work never would have been finished if not for the crew that aided in fixing up the lab. Aaron, Jeff, Dan, Laura and Ryan, thank you for making sure I didn't electrocute myself with old circuitry or get stuck in the sump. Nancy Qvale, thank you for always helping me figure out who to talk to when something really big broke in the lab. If not for Doug Wood, the tailgate might still be stuck in the flume. Without Bob Steffes, a late Friday afternoon request for a few hundred pounds of river rock may have gone unanswered. To the members of our research group, Ian Willard, Zhimin Li, Yuqi Song, Cindy Maroney and Rusen Sinir, all of the feedback was helpful and random discussions entertaining. For letting me talk about whatever was on my mind and lending a different perspective, Beth Hartmann was invaluable. Many thanks are extended to Steven Smyth for convincing me to seriously consider graduate studies. I don't know what I would be doing if he didn't ask that one simple question – "what about that professor you won't stop talking about in my office?" For all of the distractions from the 'land of engineering,' unique perspectives on leadership, teaching and time management, Rachel Hansen and Holly Prier were the best. Cheering for the Cyclones on game days would not have been as fun without them. I would like to thank my committee, Dr. Kristie Franz and Dr. Roy Gu for their help throughout this process. To my parents, the boundless support and stories about their adventures (and mishaps) from grad school always helped me smile when something wasn't working. To my advisor, Dr. Chris Rehmann, all of the encouragement, endless questions and fun poked at me over the last few years has been a tremendously enjoyable ride. I could not have asked for a better mentor.

ABSTRACT

A method is proposed to measure the transverse mixing coefficient using an acoustic Doppler current profiler (ADCP). Comparisons between measurements from an ADCP and an acoustic Doppler velocimeter (ADV) for mean velocity, Reynolds stress and turbulent kinetic energy (TKE) are used to determine the ability of ADCPs to measure turbulence quantities. Profiles collected show the effects of beam geometry in measuring velocities. ADCP data for mean velocity and Reynolds stress are used in the proposed method for estimating transverse mixing. Empirical formulas for calculating the transverse mixing coefficient are computed using data collected from both the ADCP and ADV. The empirical estimates are compared between instruments and with the proposed method. Estimates from the proposed method show the most agreement with the estimate of Fischer et al. (1979), which is believed to be the most accurate empirical estimate for the laboratory flume.

NOTATION LIST

A	=	area of the cross section
B	=	top width of the channel
$C(x,y)$	=	concentration
c	=	depth-averaged concentration
D	=	factor of diffusion
D_x	=	streamwise mixing coefficient
D_y	=	transverse mixing coefficient
D_z	=	vertical mixing coefficient
H	=	maximum depth of the channel
$h(y)$	=	depth of the channel at transverse position y
$h(\alpha, \beta)$	=	depth as a function of the position (α, β)
K	=	dispersion coefficient
K_x	=	longitudinal dispersion coefficient
K^*	=	dimensionless dispersion coefficient
k_β	=	transverse dispersion coefficient
m	=	eigenfunction mode number for the transverse direction
m_α	=	streamwise metric coefficient
m_β	=	transverse metric coefficient
n	=	eigenfunction mode number for the vertical direction
$q(\alpha, \beta)$	=	cumulative discharge at (α, β)
r_c	=	radius of curvature
$S(x, t_i)$	=	cross-section concentration in method of moments

S_n	=	sinuosity
t	=	time
\bar{t}	=	mean time of passage
TKE	=	turbulent kinetic energy
u	=	streamwise velocity
\bar{u}	=	mean streamwise velocity
$u(y)$	=	depth-averaged velocity at transverse position y
$u(\alpha, \beta)$	=	depth-averaged velocity at (α, β)
u'	=	deviation from the average velocity
$\overline{u'^2}$	=	mean squared velocity fluctuation
u_*	=	shear velocity
u_α	=	depth averaged velocity in cumulative discharge
V_i	=	velocity into the beam for index i
V_x	=	mean velocity in streamwise direction
\bar{V}_i	=	average beam velocity for index i
\bar{V}'_i	=	average beam velocity for index i
v	=	transverse velocity
$\overline{v'^2}$	=	mean squared velocity fluctuation
w	=	vertical velocity
$\overline{w'^2}$	=	mean squared velocity fluctuation
x	=	streamwise coordinate
\bar{x}	=	centroid of spatial concentration distribution
y	=	transverse coordinate

z	=	vertical coordinate
$-\langle u'v' \rangle$	=	Reynolds shear stress
$-\langle u'w' \rangle$	=	Reynolds shear stress
$-\langle v'w' \rangle$	=	Reynolds shear stress
α	=	streamtube coordinate; 20° for beam orientation
β	=	streamtube coordinate; 45° for beam orientation
κ	=	von Karman's constant
ζ	=	z/H , dimensionless vertical coordinate
η	=	y/B , dimensionless transverse coordinate
σ_t	=	temporal variance in method of moments
σ_x	=	longitudinal variance in method of moments
τ	=	time variable of integration
ν_t	=	eddy viscosity
$\partial \bar{u} / \partial y$	=	time-averaged velocity gradient
$\partial \bar{v} / \partial x$	=	time-averaged velocity gradient

CHAPTER 1: INTRODUCTION

Significance

Understanding how contaminants spread is important in predicting concentrations at various points along a waterway. Concentration estimates are often used by utilities that interact with water supplies, such as drinking water treatment plants, to refine how water is treated. Accurate estimates lead to more effective ways of handling source water, which typically lower costs. An important component of these estimates is the dispersion coefficient. The dispersion coefficient can be determined with a number of different methods. Tracer, or dye, studies are often used to gather concentration curves that are used to estimate dispersion. However, these studies are both time and money intensive, and they provide reliable estimates only for the specific flow that was measured. Empirical formulas have been developed to try and quantify dispersion, but their estimates can span an order of magnitude or more. Alternatively, the dispersion coefficient can be determined from theory. This method relies on velocity profile, geometry, and transverse mixing coefficient input. Acoustic Doppler current profilers (ADCPs) allow for both the velocity profile and geometry to be determined quickly. Using ADCPs to measure the dispersion coefficient has been tested previously, and researchers agree that ADCPs do have potential to provide quick, reasonable estimates (Bogle 1997, Carr & Rehmann 2007, Shen et al. 2010, Kim 2012). The methods behind proving the accuracy of the ADCP method are still debated however. The ability of ADCPs to specifically measure the transverse mixing coefficient has not been tested. Many empirical relations exist for the transverse mixing coefficient, but each is based on a specific dataset and likely bias towards that specific set. Accurate

measurements of turbulence with ADCPs can improve estimates of the transverse mixing coefficient and help in calculating the dispersion coefficient by theory.

Objectives

The objectives of this work are to (i) compare mean velocities measured by both an ADV and ADCP; (ii) compare turbulence quantities measured by both a Nortek acoustic Doppler velocimeter (ADV) and Teledyne StreamPro acoustic Doppler current profiler (ADCP); and (iii) assess the ability of an ADCP in measuring the transverse mixing coefficient and the dispersion coefficient.

The mean velocities will be measured by both an ADV, which is recognized as providing 'true' velocity and turbulence quantities (Voulgaris and Trowbridge, 1998), and an ADCP. . Mean velocity, Reynolds stresses, and turbulent kinetic energy (TKE) will be measured with both devices for two flow conditions and compared. The data from the turbulence quantities will be used to assess the ability of the ADCP to measure the transverse mixing coefficient and dispersion coefficient. Estimates for the transverse mixing coefficient and dispersion coefficient will be calculated using existing empirical relations and compared with the ADCP measurements.

Hypothesis

The mean velocities measured by the ADV and ADCP will match best when the width/depth (H/B) ratio is not larger than 0.5. Ratios larger than this will have additional interference with the ADCP signal, leading to less accurate measurements. Turbulence quantities measured by each will show the most agreement when the H/B ratio is once

again not more than 0.5. The estimate for transverse mixing will match empirical estimates derived in a straight laboratory flume.

Outline

This work presents background on shear dispersion theory and previous attempts at applying theory to ADCP measurements, methods for estimating the mixing coefficient and potential shortcomings, and the ability of ADCPs to measure turbulence quantities in Chapter 2. The equipment used, experimental design, and methods will be discussed in detail in Chapter 3. Chapter 4 will highlight the results of measurements of mean velocities and turbulence quantities. Discussion of these results and recommendations on the future of ADCPs in dispersion measurements will be provided in Chapter 5.

CHAPTER 2: BACKGROUND

Importance

Predicting the transport of contaminants in channels has many important applications. For example, effective treatment of drinking water requires an understanding of the input water chemistry. If a chemical is spilled at a location upstream, knowledge of the transport process is useful in determining the time at which the chemical will reach this downstream location and the concentrations the site will experience. Accurate estimates enable effective responses, which in turn reduce costs. Having a fairly quick process that provides a reliable, accurate estimate is an invaluable tool in rapid response or emergency situations. This chapter explores current methods for measuring and estimating both the mixing and dispersion coefficients, shear dispersion theory, and current applications of ADCPs to measuring dispersion. Previous work on the abilities and limitations of ADCPs in turbulent applications is also discussed.

Methods for Measuring and Estimating the Dispersion and Mixing Coefficients

Both the dispersion and mixing coefficient can be measured or estimated through a variety of ways. Currently, the most common method for calculating dispersion relies on field measurements, or dye studies. As with the dispersion coefficient, the mixing coefficient can be measured through dye studies. Additionally, attempts have been made to characterize mixing with both streamtube models and through laboratory tests. If concentration data is unavailable, both dispersion and mixing can be estimated using any number of empirical equations. These formulas provide a wide array of estimates, and they

are often times developed on a limited data set. This subsection explores the current methods for both measuring and estimating the dispersion and mixing coefficients.

Measuring the Dispersion Coefficient

The dispersion coefficient, K , has often been measured using tracer, or dye, studies. These studies are both costly and time intensive. A single injection can require a full day of monitoring instruments and collecting data. Furthermore, the data collected are only valid for that specific flow, making application very narrow. Multiple team members are required to have a successful injection, quickly multiplying the hours needed. Tracer studies require significant planning and preparation, all of which can be undone by a single day of poor weather. Permissions must be granted by local authorities, and equipment must be prepared. If an event occurs during the study that disrupts data collection, the entire planning, preparation and collection process may need to be repeated. Data collected post-disruption may be useless, and the effort may prove a waste.

However, after a successful dye study, the data gathered can be processed in multiple ways, with two common and accepted methods being the method of moments and the routing method (Rutherford, 1994, p. 213). The accuracy of these methods relies on the accuracy of the input data. Field data are often far from ideal, which can make interpreting results difficult.

Rutherford (1994, pp. 269-270) described the method of moments based on the relationship between the dispersion coefficient, K_x , and the longitudinal variance, σ_x ,

$$K_x = \frac{1}{2} \frac{d\sigma_x^2}{dt} \quad (1)$$

where t denotes time and σ_x is defined as

$$\sigma_x^2(t_i) = \frac{\int_{x=-\infty}^{\infty} [x - \bar{x}(t_i)]^2 S(x, t_i) dx}{\int_{x=-\infty}^{\infty} S(x, t_i) dx} \quad (2)$$

where x is streamwise position, the function $S(x, t_i)$ denotes the cross-sectional concentration and \bar{x} is the centroid of the spatial distribution. Concentration profiles in space are not often obtained in the field, and as such, an expression for K_x based on the temporal curves proves more useful. An alternative expression for K_x is

$$K_x = \frac{1}{2} V_x^2 \frac{\sigma_t^2(x_2) - \sigma_t^2(x_1)}{\bar{t}_2 - \bar{t}_1} \quad (3)$$

where V_x is the mean velocity between two sites (x_1 and x_2) and σ_t is

$$\sigma_t^2(x_i) = \frac{\int_{t=-\infty}^{\infty} (t - \bar{t}_i)^2 S(x_i, t) dt}{\int_{t=-\infty}^{\infty} S(x_i, t) dt} \quad (4)$$

where \bar{t}_i is the centroid of the temporal distribution. Concentration with respect to time, a much easier quantity to measure in the field, can be used to predict K_x . However, Rutherford expressed hesitations with the method of moments. Logistics and measurement errors were highlighted specifically. Collecting a complete dataset takes a significant amount of time to be done correctly. Time can be a logistical constraint, and if not enough is available, this method can be inaccurate. Measurement errors, especially in low concentrations, can greatly alter the shape of the concentration curve. This change propagates to the variance, and it eventually is reflected in the end dispersion estimate.

The routing method was emphasized as the preferred method by Rutherford. In this method, the dye cloud is measured at two locations. The cloud from the upstream location is routed to the downstream location using either the frozen cloud approximation or the Hayami solution. The frozen cloud approximation takes the temporal curve and “freezes” it before moving downstream. Rutherford (1994, pp. 213-214) summarized this with the equation

$$C(x_2, t) = \int_{\tau=-\infty}^{\infty} \frac{C(x_1, \tau)}{\sqrt{4\pi K_x (\bar{t}_2 - \bar{t}_1)}} \exp\left(-\frac{V_x^2 (\bar{t}_2 - \bar{t}_1 - t + \tau)^2}{4K_x (\bar{t}_2 - \bar{t}_1)}\right) d\tau \quad (5)$$

where $C(x, t)$ is the concentration at a time at either the upstream site (1) or downstream site (2); \bar{t} is the mean time of passage for the upstream site (1) or downstream site (2); and τ is a time variable to be used in integration. The Hayami solution (Rutherford, 1994, pp. 214-215) is slightly different, using superposition to move the cloud downstream. This is summarized as

$$C(x_2, t) = \int_{\tau=-\infty}^{\infty} \frac{C(x_1, \tau)(x_2 - x_1)}{(t - \tau)\sqrt{4\pi K_x (t - \tau)}} \exp\left(-\frac{[x_2 - x_1 - V_x (t - \tau)]^2}{4K_x (t - \tau)}\right) d\tau \quad (6)$$

Rutherford highlighted the lack of using the frozen cloud approximation as a key advantage of the Hayami solution.

For both routing methods, measurements from the downstream location are compared with the predicted values from routing. Corrections can fairly easily be made based on the stability of the tracer to satisfy conservation of mass and account for adsorption, decay, or other loss of tracer in the channel. The mean velocity and dispersion coefficient are estimated from the differences between the routing predictions and the measured concentrations.

If a dye study is not feasible, the dispersion coefficient can be calculated from other channel information. As previously discussed, the dispersion coefficient can be calculated from velocity and geometry data using ideas from shear dispersion theory. Additionally, dispersion can be calculated using any of a number of empirical equations (Table 1). As will be discussed later, there are similar limitations between empirical solutions for the dispersion and mixing coefficients. Each empirical solution was developed using a certain dataset, which can lead to solutions that are accurate for only certain situations. For the same channel with the same velocity profile, the empirical estimates vary over at least an order of magnitude. While this is not a bad method for dispersion modeling, there much room for improvement.

Table 1 – Selection of empirical equations for estimating the dispersion coefficient

Source	Formula
Fischer (1975)	$\frac{K}{u_*H} = 0.011 \left(\frac{\bar{u}}{u_*} \right)^2 \left(\frac{B}{H} \right)^2$
Liu (1977)	$\frac{K}{u_*H} = 0.18 \left(\frac{\bar{u}}{u_*} \right)^{0.5} \left(\frac{B}{H} \right)^2$
Iwasa and Aya (1991)	$\frac{K}{u_*H} = 2.0 \left(\frac{B}{H} \right)^{1.5}$
Seo and Cheong (1998)	$\frac{K}{u_*H} = 5.92 \left(\frac{\bar{u}}{u_*} \right)^{1.43} \left(\frac{B}{H} \right)^{0.62}$
Koussis and Rodriguez-Mirasol (1998)	$\frac{K}{u_*H} = 0.6 \left(\frac{B}{H} \right)^2$

Measuring the Transverse Mixing Coefficient

Methods for measuring the transverse mixing coefficient, D_y , are less common in literature compared to the dispersion coefficient (Rutherford 1994, p. 95). Similar to

dispersion, time, money and accuracy are issues that need to be addressed. No one method seems to be widely accepted.

Mixing has been measured in the lab setting, but this can rely on near ideal conditions, which are nearly the opposite of field conditions. The theoretical relationship

$$\frac{D_y}{u_* H} = \frac{0.25}{\kappa^5} \left(\frac{\bar{u} H}{u_* r_c} \right)^2 \quad (7)$$

where κ is von Karman's constant and r_c is the radius of curvature, was proposed by Fischer (1969). This relationship fit well with lab measurements but significantly underestimated values in field applications (Rutherford, 1994, p. 113).

In an attempt to better handle the changing geometry and velocity profiles in the field, one is directed to the streamtube model (Yotsukura and Sayre, 1976). Coordinates in the streamtube model are transformed from standard Cartesian coordinates to ones that mimic the depth averaged velocity lines. These coordinates, α (parallel to streamlines) and β (perpendicular to α), allow the spread of a tracer to be determined across the channel. The concept of cumulative discharge comes from this model and allows for simplifications to be made. Cumulative discharge is defined as

$$q(\alpha, \beta) = \int_{\beta'=-\infty}^{\beta} m_{\beta} h(\alpha, \beta) u(\alpha, \beta) d\beta' \quad (8)$$

where m_{β} is a transverse metric coefficient, often between 0.8 and 1.2 (Rutherford, 1994, p. 50), $h(\alpha, \beta)$ is the depth, and $u(\alpha, \beta)$ is the depth-averaged velocity. For a steady injection, the model becomes

$$\frac{\partial c}{\partial \alpha} = \frac{\partial}{\partial q} \left(D(\alpha, q) \frac{\partial c}{\partial q} \right) \quad (9)$$

where c is the depth-averaged concentration and D is the factor of diffusion, which is defined as

$$D(\alpha, q) = m_\alpha h^2 u_\alpha k_\beta \quad (10)$$

where m_α is a streamwise metric coefficient, similar to m_β ; u_α is the depth averaged velocity; and k_β is the transverse dispersion coefficient.

Cumulative discharge and the streamtube model appear in multiple works to measure transverse mixing with tracer studies (Boxall and Guymmer, 2003; Zhang and Zhu, 2011). For both of these studies, samples were taken at multiple points in the cross section, and a continuous injection of dye was used. This method, while able to handle uneven channel geometries, can be difficult to use. Cumulative discharge is fairly easy to measure with ADCPs or other simple methods. The key challenge is found in measuring the concentration profile with respect to cumulative discharge. This requires taking multiple samples within a single cross section, as was done by previous researchers. In larger rivers, it may not be possible to take samples without disturbing the flow, as would happen with boat use. A continuous injection would be needed if samples in the cross section were taken at different times, which can become costly. Otherwise, an extensive, and likely expensive, sampling network capable of taking multiple samples at the same time in different locations would be needed.

Empirical Estimates for Mixing and their Shortcomings

Many empirical estimates for the transverse mixing coefficient have been developed over the years (Table 2). These formulas, all of which were based on a specific dataset, provide a wide array of estimates. When estimating for a channel, the most accurate estimate to use could arguably be the one that was developed under similar conditions as the channel in question, such as straight compared to meandering, or field data based compared to lab data. Parameters, such as sinuosity, can be used to classify channels, but a certain amount of subjectivity remains in determining if values match original conditions.

Table 2 - Selection of empirical estimates for the transverse mixing coefficient

Source	Formula
Bansal (1971)	$\frac{D_y}{u_* H} = 0.002 \left(\frac{B}{H} \right)^{1.5}$
Yotsukura and Sayre (1976)	$\frac{D_y}{u_* H} = 0.4 \left(\frac{\bar{u} B}{u_* r_c} \right)^2$
Sayre (1979)	$\frac{D_y}{u_* H} = (0.3 - 0.9) \left(\frac{\bar{u} B}{u_* r_c} \right)^2$
Fischer et al. (1979)—straight	$\frac{D_y}{u_* H} = 0.15$
Fischer et al. (1979)—gently meandering	$\frac{D_y}{u_* H} = 0.6$
Deng et al. (2001)	$\frac{D_y}{u_* H} = 0.145 + \frac{1}{3,520} \left(\frac{\bar{u}}{u_*} \right) \left(\frac{B}{H} \right)^{1.38}$
Jeon et al. (2007)	$\frac{D_y}{u_* H} = 0.03 \left(\frac{\bar{u}}{u_*} \right)^{0.46} \left(\frac{B}{H} \right)^{0.30} S_n^{0.73}$

If all estimates are applied to the channel to gain insight into the range of mixing, a variety of solutions are obtained. The most comprehensive answer would be one that fits in two categories for being conservative – conservative with respect to the time of arrival and conservative with respect to the peak concentration. Each empirical formula for the

mixing coefficient provides a different estimate, which leads to estimates for dispersion to each be different. The solution which predicts the earliest arrival (and likely latest departure) can be used to estimate the time a pollutant would be passing by. Combining the estimate which predicts the largest concentration with the estimate that gives the largest time of passage would provide the most comprehensive answer.

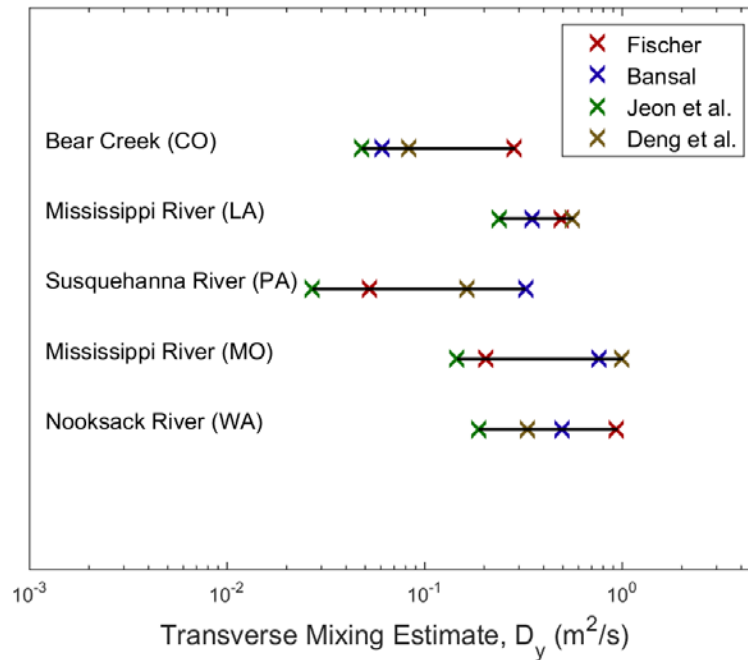


Figure 1 - Range of transverse mixing coefficient for five different locations. The dataset for each location was processed using four standard empirical equations. Data from Nordin and Sabol (1974), McQuivey and Keefer (1974), Rutherford (1994), and Seo and Cheong (1998)

There are difficulties when assessing how realistic each formula estimates mixing. The formulas in Table 2 vary over an order of magnitude, or more (Figure 1), for the same input information. The uncertainty that comes with an order of magnitude is huge, and it is relevant when a large uncertainty equals a large cost. Reducing the uncertainty from an order of magnitude to a factor of 2 or 3 would be significant improvement.

ADCP Method of Measuring the Dispersion Coefficient

Acoustic Doppler current profilers (ADCPs) are a relatively young technology, with the first versions produced in the early 1980's (Simpson, 2001). These instruments make it easy to measure velocity profiles and channel geometry, both of which are key components in determining dispersion. The use of ADCPs by organizations such as the United States Geological Survey in discharge and velocity measurements is widespread. Gaining information on a water quality parameter from these instruments is a benefit that would replace the inefficient, time consuming tracer methods with an efficient, quick measurement, especially when short time frames are required. Accuracy in measuring turbulence allows for all parameters needed to compute the dispersion coefficient to be measured, removing the need to make assumptions and apply empirical equations. This sub-section will focus on shear dispersion theory, examples of using ADCPs to measure the dispersion coefficient, and the current drawbacks associated with computing dispersion.

Brief Introduction to Shear Dispersion Theory

The classical equation used for describing contaminant transport uses geometric and stream based data combined with properties unique to the channel to determine concentrations and spreading. The three dimensional advection-diffusion equation is

$$\frac{\partial C}{\partial t} + u \frac{\partial C}{\partial x} = \frac{\partial}{\partial x} \left(D_x \frac{\partial C}{\partial x} \right) + \frac{\partial}{\partial y} \left(D_y \frac{\partial C}{\partial y} \right) + \frac{\partial}{\partial z} \left(D_z \frac{\partial C}{\partial z} \right) \quad (11)$$

where C is the concentration; u is the velocity; x , y , and z are the streamwise, transverse, and vertical coordinates; and D_x , D_y and D_z are the mixing coefficients in the streamwise, transverse and vertical directions. The dimensionless dispersion coefficient, $K^* = KD_y \sqrt{u^2 B}$,

which accounts for variations from both vertical and transverse velocity gradients, can be defined as

$$\begin{aligned}
K^* = & \frac{2}{\pi} \sum_{m=1}^{\infty} \frac{1}{m^2} \left[\int_0^1 \int_0^1 \frac{u'(\eta, \zeta)}{\bar{u}} \cos(m\pi\eta) d\eta d\zeta \right]^2 \\
& + \frac{2\tau}{\pi^2} \sum_{n=1}^{\infty} \frac{1}{n^2} \left[\int_0^1 \int_0^1 \frac{u'(\eta, \zeta)}{\bar{u}} \cos(n\pi\zeta) d\eta d\zeta \right]^2 \\
& + \frac{4}{\pi^2} \sum_{n=1}^{\infty} \sum_{m=1}^{\infty} \frac{1}{m^2 + \tau^{-1}n^2} \left[\int_0^1 \int_0^1 \frac{u'(\eta, \zeta)}{\bar{u}} \cos(m\pi\eta) \cos(n\pi\zeta) d\eta d\zeta \right]^2
\end{aligned} \tag{12}$$

where $\eta=y/B$, or a non-dimensional transverse coordinate, and $\zeta=z/H$, or a non-dimensional vertical coordinate and m and n are eigenfunction mode numbers (Schwab and Rehmann, 2015). The first term in (12) represents contributions from the transverse gradient, while the second represents contributions from the vertical gradient. The third term represents the combined effects of both the transverse and vertical gradient. Contributions from the third term are nearly always negligible, while the second term rarely contributes (Schwab and Rehmann, 2015, Appendix A). This analysis confirms that the analysis of Fischer et al. (1979) can be considered accurate for a vast majority of channels. The definition of the dispersion coefficient that evolves from this analysis and is commonly used in ADCP applications is

$$K = \frac{-1}{A} \int_0^B u(y)h(y) \int_0^y \frac{1}{D_y h(y)} \int_0^y u(y)h(y) dy dy dy \tag{13}$$

where A is the area of the cross section; u is the depth-averaged velocity; and h is the depth. All quantities, aside from the mixing coefficient, D_y , can be easily measured or computed.

Examples of ADCPs in Measuring the Dispersion Coefficient

The application of ADCPs to dispersion measurements has been suggested and studied by previous researchers. Bogle (1997) worked with published results of velocity and geometry data. These data were collected with ADCPs in the Sacramento and Old Rivers. The profiles were fit to equations that could be processed using Fischer's classic method of calculating dispersion. It was noted that uncertainty does appear in these measurements due to the nature of ADCPs. Because of interference, the instruments cannot measure all the way to the surface or banks, and leaves a small gap of missing data. Bogle handled these gaps with a linear extrapolation. Velocities at the bottom and side boundaries were set to zero. Logarithmic curves were fit to vertical velocity profiles, while the transverse profiles were fit with quartic curves. Differences of an order of magnitude were observed between dispersion values calculated with ADCP velocity profiles and empirical estimates. Bogle concluded that more testing was needed and that possible error was due to the idealized conditions Fischer developed his empirical relationship under.

ADCPs measurements were paired with dye study data by Carr and Rehmann (2007). Ten different locations were investigated. Unmeasured regions were handled with a variety of methods following suggestions by prior researchers, including Bogle (1997). The effect of the unmeasured regions were further investigated. Synthetic profiles were created that extended to the boundaries, and the dispersion coefficient was calculated. Data were removed, and the gaps created were replaced using methods applied to ADCP field data. Not surprisingly, the larger the boundary gaps were, the larger the discrepancy between the original and new values for the dispersion coefficient. Overall accuracy of the ADCP method was linked to profile shape (uniform compared to varying), reach

consistency, and recirculation zones. They concluded that for many channels, ADCPs can estimate the dispersion coefficient within a factor of 3. This is a significant improvement on the order of magnitude range that empirical formulas can produce.

Applying ADCPs to dispersion was expanded on by Shen et al. (2010), as they collected dye study data and ADCP transects simultaneously. They argued that ADCP data and dye study data must be collected simultaneously, or at least within close proximity to each other to have meaningful results. Raw velocity data was manipulated with both power law and logarithmic profiles to fill in missing bins. The velocity profile was oriented in two different directions – one that was streamwise and one that was perpendicular to the transect line. They identified six separate cases for estimating the dispersion coefficient with ADCPs based on combinations of velocity smoothing and orientation and identified the error compared to tracer data for each (Table 3). Consistency of the method is clearly better for velocities that are oriented normal to the transect line. However, streamwise oriented velocities show promise as the lower bounds are closest to the tracer estimates.

Table 3 - Processing combinations and error bounds estimated from Figure 4 of Shen et al. (2010)

Method	Velocity Smoothing	Velocity Orientation	Error	
			Low	High
1	Logarithmic Law	Streamwise	2%	300%
2	Logarithmic Law	Normal to Transect	30%	200%
3	Power Law	Streamwise	2%	300%
4	Power Law	Normal to Transect	30%	200%
5	No Smoothing	Streamwise	2%	300%
6	No Smoothing	Normal to Transect	30%	200%

More recently, Kim (2012) tested ADCPs in a large river context. Kim used AdcpXP, a program designed to work with ADCPs and compute various quantities from collected data, with the measurements to compute the dispersion coefficient due to both

vertical and transverse shear. A curious point in this work is the sentiment that missing data at the banks is negligible and can be neglected when computing the dispersion coefficient. This seems counterintuitive, as dispersion is often driven by the velocity gradient, which is larger near the banks than in the middle of the channel. This also opposes what has been hinted at by previous researchers (Bogle, 1997; Carr and Rehmann, 2007; Shen et. al 2010). Kim handled missing data near the surface and bottom of the channel with logarithmic law, which is in line with previous work. The dispersion coefficient was calculated using many empirical equations and compared with the values produced by the ADCP measurements. The empirical equations were suggested to overestimate the actual value of the dispersion coefficient. With the lack of dye study data, it is difficult to say for certain that the empirical equations overestimated the actual value. It is possible that the ADCP values were low estimates. Without solid identification of the actual value of the dispersion coefficient, it is difficult to get a feel for how much improvement this method provides. Other mechanisms besides shear dispersion, such as secondary currents, often contribute to the spread of contaminants. If only the effects of shear dispersion are measured by ADCPs in a channel where multiple mechanisms are contributing to spreading, the estimate will be lower than the actual value.

The Mixing Coefficient as a Limitation

ADCPs have the ability to measure many quantities important in calculating the dispersion coefficient. However, an accurate and consistent method for handling the mixing coefficient in (13) has yet to be determined. Typically, this value is determined using one or more empirical formulas. Each formula was tailored to fit a specific stream

and dataset and likely shows bias towards the behavior of that stream and dataset. This wide array of formulas produces an equally wide range of values, which affects the total dispersion calculation. Current methods for measuring and estimating the mixing coefficient will be discussed in detail in the next section.

The Ability of the ADCP to Measure Mean Velocity and Turbulence

Before ADCPs can be relied on for measuring turbulence quantities, an understanding of the accuracy must be obtained. Various models of ADCPs have been tested for accuracy (Gargett, 1994; Stacey et al., 1999; Nystrom et al., 2007). Previously, researchers have tested ADCPs that were mounted on a fixed frame or used on a ship in a coastal or tidal application. Testing for turbulence using float mounted ADCPs designed for river measurements have not been widely published.

One benchmark for comparing ADCP measurements is the acoustic Doppler velocimeter (ADV). Voulgaris and Trowbridge (1998) tested the ability of ADVs to measure true flow quantities. A laser Doppler velocimeter was used to provide a second, independent set of measurements in addition to the ADV measurements. Measured quantities were compared to empirical and theoretical estimates for expected values. The ADV was found to measure within 1% for both mean velocity and Reynolds stress. Due to differences in how ADVs and ADCPs record measurements, a few assumptions must be made regarding homogeneity in the calculation of turbulence values using ADCPs. These assumptions constitute a large part of the uncertainty surrounding the accuracy of ADCPs in turbulence measurements and will be discussed further in Chapter 3.

One of the first researchers to explore using ADCPs in a “nonstandard way” was Gargett (1994). Various turbulence quantities were observed, including turbulent kinetic energy and Reynolds stresses. One of the highlighted points was the importance of a stable platform to improve accuracy of measurements. Techniques for extracting velocities and Reynolds stresses from ADCP measurements were described in detail by Stacey et al. (1999). Measurements taken with ADCPs were once again found to compare well with theory. While neither of these works measured in a river type flow or with instruments designed to be used in a standard float, they are important in identifying the potential of acoustic techniques in measuring turbulent flow fields.

More recently, Nystrom et al. (2007) tested two different ADCP models, a three-beam Nortek ADCP and a four-beam RD Instruments Rio Grande ADCP. Both instruments were mounted on a stationary platform in a flume for testing. The four-beam ADCP handled well, and produced accurate mean velocity and Reynolds stress profiles when compared to ADV measurements. Reproduction of profiles using the three-beam ADCP was more successful in flows exhibiting weaker turbulence. Results were compared with ADV measurements, and continued testing of ADCPs are recommended to further increase confidence in the instrument.

Research using float mounted ADCPs that measure with the transducer mounted in the float is significantly less. The RD Instruments Teledyne StreamPro ADCP float is a model commonly used by organizations such as the USGS for discharge measurements. The ability to gain an insight into mixing from these already existing measurements provides significant value and reduces the expenses incurred when going and solving for these quantities directly.

Importance of Statistical Homogeneity and Stationarity

Assuming instantaneous homogeneity in a turbulent flow would be incorrect. Assuming the statistical values of that same turbulent flow are the same is more plausible. The significance of statistical homogeneity, which is a large component of why ADCP values are being tested and compared to the ADV, is due to the way ADCPs measure velocity. The geometry of the ADCP beam configuration forces the instrument to measure velocities at different locations in the flow. Each beam will experience slightly different velocities, and most certainly will not experience identical fluctuations at identical points in time. Additionally, as the beams collect data from locations farther from the transducer, the distance between beams will increase, further reducing the chance that the same conditions at the same time are observed. Statistical stationarity appears in the collection methods for both ADV and ADCP data. For data collection, both instruments were centered over the same location. To accomplish this, the sampling times needed to be offset. As the interest in the ADCP data is in the statistics of the flow, not the instantaneous quantities, this method was acceptable.

Summary

Current methods used for measuring and estimating the dispersion coefficient have significant room for improvement. Dye studies are used commonly to measure dispersion in natural channels. These studies are costly in both the monetary and time senses, and they have a narrow application. Empirical estimates have been developed to try and quantify dispersion based on measurable quantities, such as velocity and geometry, but these

estimates produce a wide array of values. Selecting an appropriate estimate for each situation is challenging, and there is not a clear method for doing so.

More recently, shear dispersion has been used in calculating the dispersion coefficient. Fischer's analysis produced an equation for the dispersion coefficient that is dependent on three main quantities – the velocity profile, geometry and transverse mixing coefficient. Instrument advances have made detailed measurements of both velocity profiles and geometry easier to acquire. The only remaining quantity that requires attention is the mixing coefficient.

Measuring the dispersion coefficient with data collected from acoustic Doppler current profilers has shown promise. These methods allow for faster and less expensive estimates of dispersion. Additionally, because of the efficiency of ADCPs, many different flows can be measured with a significantly shorter planning period. Attempts to measure dispersion all have one common flaw in how the mixing coefficient is treated. No standard method has been developed yet for handling this parameter. Methods for measuring and estimating the mixing coefficient have similar downfalls as the dispersion coefficient. Dye studies are costly, and empirical formulas vary over an order of magnitude or greater. Without a consistent method for measuring the mixing coefficient, consistency in the dispersion coefficient cannot be achieved.

In natural channels, mixing can be quantified through measurements of turbulence quantities. Using ADCPs to measure these quantities has been evaluated in the past. Previously, researchers have focused on coastal or estuarine measurements with ADCPs. Measurements in open channel flows are significantly less, with research using ADCPs mounted on a stationary frame. Mounting the ADCP in the designed float has not been

tested for accuracy. Results have indicated that there is promise for the ADCP to measure turbulence quantities.

Assessing the ability of the StreamPro ADCP to measure turbulence is the foundation for developing a consistent method for measuring the dispersion and mixing coefficient with ADCPs.

CHAPTER 3: METHODS

This section is designed so that another user can duplicate these experiments. The equipment used for each of experiments is detailed. Procedures used to determine sample time is covered. Lastly, the methods used in processing are explained. Additionally, the MATLAB codes used in processing can be found in Appendix B.

Experimental Facility

Experiments were conducted in the hydraulics lab in Town Engineering Building at Iowa State University. A Plexiglas flume 60.96 cm wide with 60.96 cm sidewalls was used for the experiments (Figure 2). The length from headgate to tailgate was 9.14 m. A polycarbonate tailgate was used to control the depth of the water in the flume, typically up to 40 cm. Depths greater than this value did not allow time or space for water flow to be stopped before a potential overflow occurred. The head gate was raised high enough so that flow was not obstructed. A honeycomb structure sat 30 cm downstream from the headgate. The honeycomb stabilized flow and absorbed waves from bubbles at the entrance. The slope of flume was zero at the point of measurement. A slight slope existed at various points throughout the channel, but it was not uniform.

In a small channel with reflective walls, sound waves are more likely to bounce between walls and the bottom, leading to additional noise and poor quality measurements. To address this, the bottom of the flume was roughened with rock. A tarp layer was placed directly on the Plexiglas bed to protect against scratches. A layer approximately 4 cm deep of 16 mm gravel was placed on top of the tarp. This rocked area stretched from the tailgate to roughly 10 cm downstream of the honeycomb. This layer created a more accurate

representation of a natural channel bottom. Additionally the rocks served as a sound absorber, preventing excessive reflection of sound waves. The sidewalls and tailgate remained bare during the experiments.

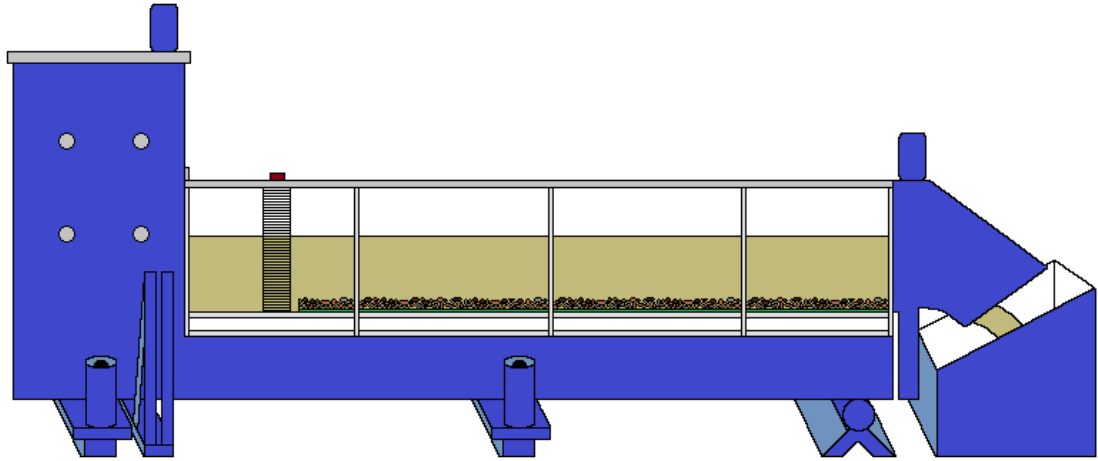


Figure 2 - Plan view of the flume

Two vertical turbine pumps pumped water from a 5.2 m deep sump to a constant head tank two floors above the lab. The smaller pump was rated at $0.019 \text{ m}^3/\text{s}$ and the larger pump at $0.032 \text{ m}^3/\text{s}$. From the constant head tank, water was directed into either the flume, a weighing tank, or partially into each. Valves along this pipe system were used to set the depth of water in the flume (Figure 3). As a higher percentage of water was diverted into the weighing tank, the water level in the flume would decrease. Similarly, when less water was diverted into the weighing tank, the water level in the flume increased. Large bubbles often came out of the entrance to the flume. These were minimized by small adjustments made at various points throughout the system. No specific combination of valve settings appeared to be immune to these bubbles. The flume was monitored during start up for bubbles. All adjustments in an attempt to eliminate bubbles were made before measurements started.

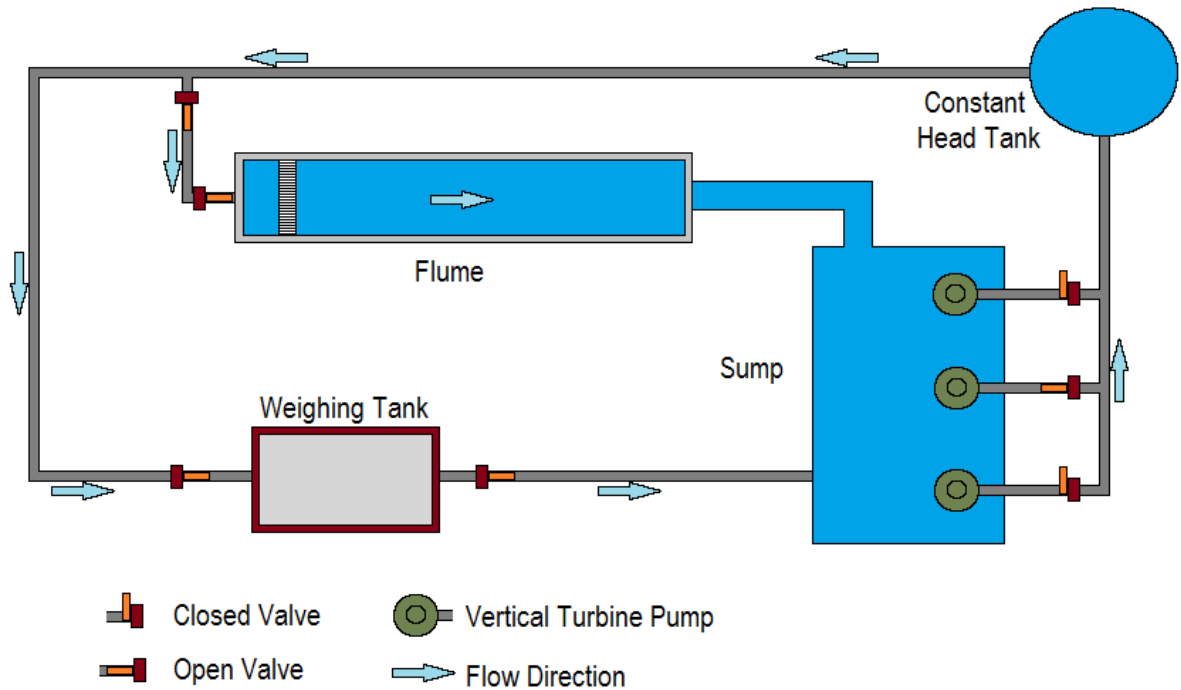


Figure 3 - Pump & flume system schematic

Equipment

The two instruments used in collecting data were a Teledyne RDI StreamPro ADCP and a Nortek ADV. The basic principle behind both the ADCP and ADV is the Doppler effect. Both instruments send sound pulses to a sample volume of water some distance from the transducer. Those pulses bounce off suspended material in the water and return to receivers. The perceived change in frequency is used by the instrument to calculate a velocity. An important assumption with acoustic based instruments is that materials suspended in the water are moving at the same speed as the water (Teledyne, 2011). For these experiments, a fine reddish brown soil was present in the water and provided plenty of suspended material for a good quality signal.

RD Instruments StreamPro Acoustic Doppler Current Profiler

The StreamPro ADCP was the instrument to be tested for this study. An ADCP has four transducers, each of which emits a pulse of sound (Figure 4). Each transducer receives the pulses with shifted frequencies. The ADCP measures at multiple depths simultaneously. Received data is broken up using a process known as range-gating to develop the velocity profile across the entire depth (Teledyne, 2011). Far away locations (for this test, a greater depth) require more time for the signal to return. Likewise, locations close to the transducer require less time. The ADCP processes these delays in response time and associates each frequency shift, or velocity, with a depth. This allows for an entire velocity profile to be determined much more quickly than with the ADV.

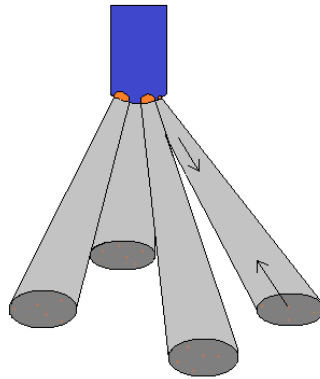


Figure 4 - RD Instruments StreamPro ADCP Schematic

The ADCP was launched in the flume in the field housing and float. Using the entire float apparatus provides some consistency between field and laboratory measurement conditions. The transducer was mounted in the boom in the extended position. This allowed for more accurate and sensitive measurements (Figure 5, StreamPro Manual). Beam orientation of 45° matched the requirements in the ADCP manual (Figure 5). Measurements within 5 cm of the surface were not collected due to the blanking distance

and transducer submergence depth, and measurements within 6% of the bottom were marked as bad due to side-lobe interference (Simpson, 2001).

The float was held stationary by two control points. Streamwise position was maintained by looping the ring at the end of the tow arm on a rod fixed to the frame of the flume. Transverse position was maintained with two guide rulers attached to the flume frame. The rulers were positioned parallel to the streamwise direction and allowed the transducer to float freely on the water surface while preventing drifting greater than 5 mm from the center of the channel.

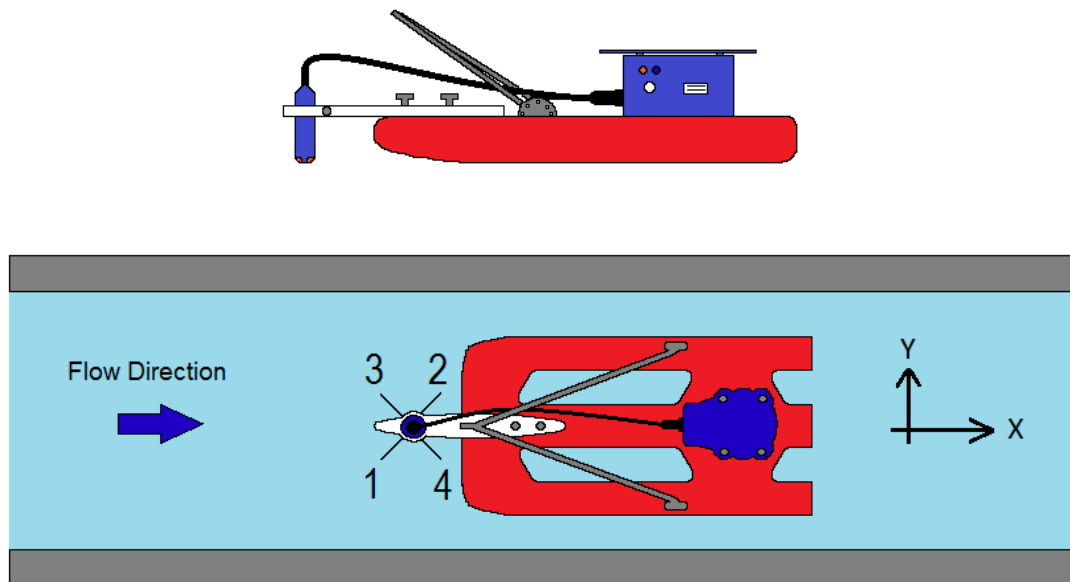


Figure 5 – StreamPro transducer mounting position (top); Instrument and beam orientation (bottom)

WinRiver II was used with a bluetooth connection to control the ADCP and collect data. Input data values are shown in Table 4. The maximum water depth value for rough initial setup was selected based on a measurement tape adhered to the side of the flume. Maximum water speeds were determined using the ADV before any data collection and recording began. The boat speed was set to zero as the float was stationary for testing and the transducer depth was held consistent throughout all tests. No reference was used for

velocities as the float was assumed to be stationary. Including bottom track created issues with data quality as the bottom ping was reverberating throughout the channel, returning widely inconsistent values (Teledyne, personal communication). This is visually observed in the intensity profile when pinging is occurring.

Table 4 - WinRiver II measurement wizard settings

Value	Test 1	Test 2
Transducer Depth (m)	0.02	0.02
Max. Water Depth (m)	0.33	0.33
Max. Water Speed (m/s)	0.15	0.15
Streambed	Gravel	Gravel
Water Mode	Mode 13	Mode 13

Two additional user input commands were added in the commands preview screen. The command WS1 was used to create bin sizes of 1 cm. This size bin allowed for more points to be measured in shallow flow. In a deeper channel the bin size would need to be adjusted accordingly. Beam coordinates were selected using command EX00111. Beam velocities were deconstructed and multiplied, added, and subtracted from each other to extract mean velocities and Reynolds stress profiles. Equations detailing this process are included later in this chapter in the Processing section.

Nortek Acoustic Doppler Velocimeter

A Nortek acoustic Doppler velocimeter was used as the reference instrument. ADVs have been shown to produce results that are accepted as valid truth measurements (Voulgaris and Trowbridge, 1998), making the instrument a logical choice for comparison. Unlike the ADCP, the ADV emits pulses of sound from a single central transducer and four different receivers record the shifted frequencies (Figure 6). Velocities are measured at a

single location 5 cm below the central transducer. This makes measuring a complete profile time consuming compared to the ADCP. Because the ADV measures at a depth below the sensors and the receivers and transducer must be submerged, measurements within 5 centimeters of the surface were not obtained. This was not considered a significant disadvantage as this lines up well with the blanking and transducer submergence space for the ADCP. Measurements with the ADV were obtained much closer to the bed than those with the ADCP due to the lack of side-lobe interference.

The ADV was mounted on a moveable cart sized for the top of the flume (Figure 6). The main frame carried the excess cable and supported the weight of the instrument housing. The sensor portion was tied to a point gauge allowing for easy vertical adjustments. The ADV was positioned normal to the flume bottom for all measurements.

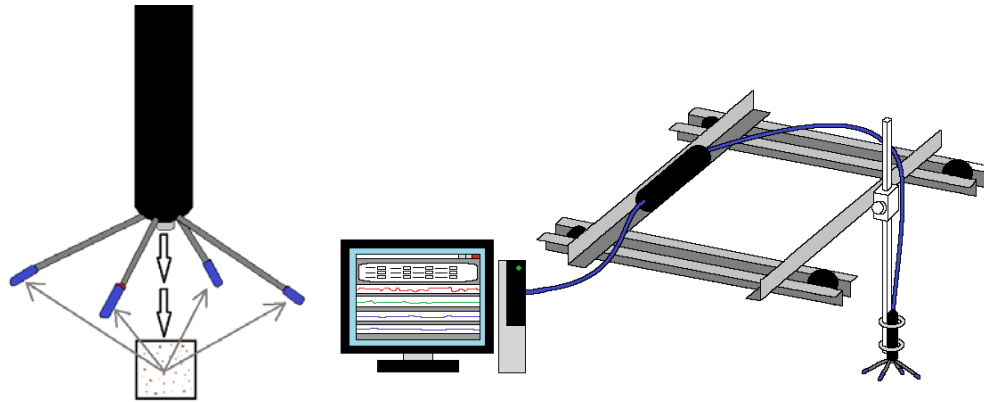


Figure 6 - Nortek ADV schematic (left); ADV mounting apparatus (right)

Nortek provides a Vectrino+ software designed to work with ADVs they produce. This software was used to control and collect data for these tests. Standard configuration input values are included in Table 5. A fast sampling rate was used for comparison measurements. Using a quick sampling rate reduced the possibility that the smallest structures did not get adequately sampled. A much smaller sampling rate was used for

stationarity tests. This is possible because the values of interest, mean velocities, are not as sensitive to sampling frequency. An added benefit of reducing the frequency for stationarity tests was a reduced volume of data, and consequently shorter time required for processing.

Table 5 - Vectrino+ software settings

Value	Test 1	Test 2	Stationarity Test
Sampling Rate (Hz)	200	200	2
Nominal Velocity Range (m/s)	+/- 0.03	+/- 0.03	+/- 0.03
Transmit Length (mm)	1.8	1.8	1.28
Sampling Volume (mm)	7.0	7.0	3.4
Power Level	HIGH	HIGH-	HIGH
Coordinate System	XYZ	XYZ	XYZ
Sampling Time (s)	300	300	5,400

Experiment Design

The important components involved with designing the experiment were sampling time, vertical resolution and equipment limits. Equipment limited both the maximum depth (flume limitation) and the minimum depth (ADCP interference). Vertical resolution was based on the capacity of the ADCP and the size of bins. Lastly, the sampling time needed to be determined before any experiments were run to ensure the data collected were useful.

The sampling time was determined by a simple scaling argument. The time scale of the largest turbulent structure in a flow was found by dividing a characteristic length by a characteristic velocity (Tennekes and Lumley, 1989, pp. 14-26). In this case, the characteristic length is the depth of flow, and the characteristic velocity is the average velocity observed. For the range of flows the flume can handle, the time scale was approximately 3 seconds. One hundred structures were sampled, leading to a minimum

sampling time of 5 minutes per vertical position for the ADV. ADCP measurements were recorded for 20 minutes.

A longer sampling time of 90 minutes was used with the ADV at one geometric location in the flow. This sample was used to establish the ability of the system to maintain a steady flow and was not used in any comparison measurements. Any large scale trends in the flow were able to be identified before data collection was started. Testing for stationarity began after all initial visual transients died out. A ruler on a side wall of the flume provided a means for visually checking stability. The time to reach a stable flow varied for each different combination of valves, but was typically no less than 30 minutes.

The vertical resolution, or number of points in the profile, was dictated by the ADCP. An ADCP collects data for all vertical positions at once, which each vertical position being a bin. The minimum size of these bins is 1 cm. The size of bin is matched to the flow depth. Too large of a bin size in a small flow does not provide the resolution required to develop an accurate profile. For these experiments, the minimum allowable bin size was used. This allowed for the finest resolution possible. Measurements were taken 4.1 m upstream of the tailgate. Both instruments were located in the center of the channel.

The two cases tested used different depths, resulting in different H/B ratios for the flow. Ratios greater than 0.5 are associated with poor measurements due to increased acoustic contamination (Teledyne, personal communication). The first case measured was a shallow, slow flow that met Teledyne recommendations with a ratio of 0.47. The second case measured was a deeper, faster flow that resulted in a ratio of 0.53, or more than the recommended 2. A larger range of flows was not possible due to the limits of the flume.

Larger depths (larger ratios) were difficult to stabilize and smaller depths lost a larger percent of the profile to a fixing instrument submergence and blanking distance.

Processing

Data files from both instruments were processed with multiple programs. Data from the ADV was collected using the Nortek provided Vectrino+ software. Within this software, data files were processed and created .vno files. These files were then processed using WinADV. WinADV filtered out spikes and excess noise and created a set of .Vf files. More information on the methods to remove spikes from ADV data can be found in Wahl (2000) and Goring and Nikora (2002). MATLAB was used to process the final data files. A series of codes matched depth information with each data file. Average velocity, velocity fluctuations, and all components of the Reynolds stress tensor were calculated through this code.

ADCP data was initially processed through WinRiverII. An ASCII output template was created specifically for these experiments. Collected transects were reprocessed with this ASCII template ON. The output text file format is summarized in Table 6. The first subscript on the bin depth refers to the ensemble the depth cell is associate with, while the second subscript is the depth location (i.e., depth cell 1, 2, 3, etc.). The beam velocity subscripts represent the beam, the ensemble and the depth cell, respectively.

Table 6 - WinRiverII output ASCII template

Ens.		Bin Depth (m)		Beam 1 Velocity (m/s)				Beam 4 Velocity (m/s)
1	\$\$	D ₁₁ , D ₁₂ , ... D _{1n}	\$\$	V ₁₁₁ , V ₁₁₂ , ... V _{11n}	\$\$...	\$\$	V ₄₁₁ , V ₄₁₂ , ... V _{41n}
2	\$\$	D ₂₁ , D ₂₂ , ... D _{2n}	\$\$	V ₁₂₁ , V ₁₂₂ , ... V _{12n}	\$\$...	\$\$	V ₄₂₁ , V ₄₂₂ , ... V _{42n}
⋮	⋮	⋮	⋮	⋮	⋮	⋮	⋮	⋮
n	\$\$	D _{n1} , D _{n2} , ... D _{nn}	\$\$	V _{1n1} , V _{1n2} , ... V _{1nn}	\$\$...	\$\$	V _{4n1} , V _{4n2} , ... V _{4nn}

The resulting ADCP output text file was processed through MATLAB. Two core utility programs were used to calculate velocities and Reynolds stresses. ADCP_read_2 was used to read in raw data from the text file. ADCP_process_f was used to process raw data and output velocity and Reynolds stress components. WinRiverII flagged bad velocity data with a -32768 value. These flags were replaced with NaNs in the reading program. No other filtering was applied. For more information on how WinRiverII determines bad velocity data, refer to the WinRiverII user manual (Teledyne, 2016).

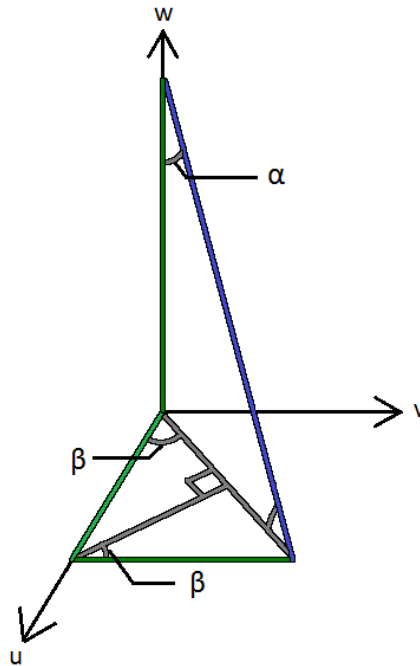


Figure 7 - Projection of ADCP beam velocity onto each axis for beam 2

Because information was stored as into the beam, calculating average values required manipulation of the original data. Each beam can be broken down into 3 segments, each consisting of a u (streamwise), v (transverse), and w (vertical) component (Figure 7).

The into beam velocity for each beam is

$$V_1 = w_1 \cos(\alpha) + u_1 \cos(\beta) \sin(\alpha) + v_1 \cos(\beta) \sin(\alpha) \quad (14)$$

$$V_2 = w_2 \cos(\alpha) - u_2 \cos(\beta) \sin(\alpha) - v_2 \cos(\beta) \sin(\alpha) \quad (15)$$

$$V_3 = w_3 \cos(\alpha) + u_3 \cos(\beta) \sin(\alpha) - v_3 \cos(\beta) \sin(\alpha) \quad (16)$$

$$V_4 = w_4 \cos(\alpha) - u_4 \cos(\beta) \sin(\alpha) + v_4 \cos(\beta) \sin(\alpha) \quad (17)$$

where V_1 , V_2 , V_3 , and V_4 are the into beam velocities. The angles α and β refer to the deviation from vertical (20°) and the transverse (45°) orientation, respectively.

Each of the average velocity components was calculated in two ways. Two groups of two beams were used for each of the calculations. For the longitudinal direction, beams 1 and 4 were a group and beams 2 and 3 were a second group. The transverse direction grouped beams 1 and 3 for the first group and beams 2 and 4 for the second group. Vertical velocities were calculated using a grouping of beams 1 and 2 or beams 3 and 4. The six expressions for the time-averaged velocities are

$$\bar{u} = \frac{\bar{V}_1 - \bar{V}_4}{2 \cos(\beta) \sin(\alpha)} = \frac{\bar{V}_3 - \bar{V}_2}{2 \cos(\beta) \sin(\alpha)} \quad (18)$$

$$\bar{v} = \frac{\bar{V}_1 - \bar{V}_3}{2 \cos(\beta) \sin(\alpha)} = \frac{\bar{V}_4 - \bar{V}_2}{2 \cos(\beta) \sin(\alpha)} \quad (19)$$

$$\bar{w} = \frac{\bar{V}_1 + \bar{V}_2}{2 \cos(\alpha)} = \frac{\bar{V}_3 + \bar{V}_4}{2 \cos(\alpha)} \quad (20)$$

where the overbar represents the time average value.

The Reynolds stress components can be extracted from the into beam data with a few manipulations. The into beam velocity fluctuation, V_i' , was calculated the same way as all previous fluctuation quantities. Analogous to the velocity components, each

Reynolds stress component was able to be calculated in two ways. Each of the six Reynolds stress components and corresponding methods for calculation are

$$-\langle u'v' \rangle = \frac{\overline{V_3'^2 - V_1'^2 + V_4'^2 - V_2'^2}}{8 \cos^2(\beta) \sin^2(\alpha)} = \frac{\overline{V_1'V_2' - V_3'V_4'}}{4 \sin^2(\alpha) \cos(\beta) \sin(\beta)} \quad (21)$$

$$-\langle u'w' \rangle = \frac{\overline{V_2'^2 - V_1'^2 + V_4'^2 - V_3'^2}}{8 \cos(\alpha) \sin(\alpha) \cos(\beta)} = \frac{\overline{V_2'V_4' - V_1'V_3'}}{4 \cos(\alpha) \sin(\alpha) \sin(\beta)} \quad (22)$$

$$-\langle v'w' \rangle = \frac{\overline{V_2'^2 - V_1'^2 + V_3'^2 - V_4'^2}}{8 \cos(\alpha) \sin(\alpha) \sin(\beta)} = \frac{\overline{V_2'V_3' - V_1'V_4'}}{4 \cos(\alpha) \sin(\alpha) \sin(\beta)} \quad (23)$$

$$\overline{u'^2} = \frac{\overline{(V_1' - V_4' + V_3' - V_2')^2}}{4 \cos^2(\beta) \sin^2(\alpha)} \quad (24)$$

$$= \frac{1}{2 \sin^2(\beta) \sin^2(\alpha)} \left(\overline{V_1'^2 - V_1'V_4'} + \frac{1}{2} \left[\overline{V_1'V_2' + V_2'V_4' - V_1'V_3' - V_3'V_4'} \right] \right)$$

$$\overline{v'^2} = \frac{\overline{(V_1' - V_3' + V_4' - V_2')^2}}{4 \cos^2(\beta) \sin^2(\alpha)} \quad (25)$$

$$= \frac{1}{2 \cos^2(\beta) \sin^2(\alpha)} \left(\overline{V_2'^2 - V_2'V_4'} + \frac{1}{2} \left[\overline{V_1'V_2' + V_1'V_4' - V_2'V_3' - V_3'V_4'} \right] \right)$$

$$\overline{w'^2} = \frac{\overline{(V_1' + V_2' + V_3' + V_4')^2}}{4 \cos^2(\alpha)} \quad (26)$$

$$= \frac{1}{2 \cos^2(\alpha)} \left(\overline{V_4'^2 + V_3'V_4'} + \frac{1}{2} \left[\overline{V_1'V_3' + V_2'V_3' - V_2'V_4' - V_1'V_4'} \right] \right)$$

where the subscript on each of the velocity components indicates the into beam velocity

used. For example, V_1V_3' is the product of the fluctuations of beams 1 and 3. Likewise, $\overline{V_1'^2}$

is the product of the fluctuations of beam 1 multiplied by itself and averaged.

Turbulent kinetic energy (TKE) was calculated using the Reynolds normal stresses computed from each instrument. Any disagreement between the ADCP and ADV should be carried through to TKE computations. TKE was computed as

$$TKE = \frac{(\overline{u'^2} + \overline{v'^2} + \overline{w'^2})}{2} \quad (27)$$

The transverse mixing coefficient was estimated using two main categories of methods. The primary proposed method relied on a relationship between eddy viscosity, ν_t , time averaged velocity and the streamwise-vertical component of Reynolds stress. The proposed method estimates the transverse mixing coefficient as approximately equal to the eddy viscosity, or

$$D_y \approx \nu_t = -\frac{-\langle u'v' \rangle}{\partial \bar{u} / \partial y + \partial \bar{v} / \partial x} \quad (28)$$

where $\partial \bar{u} / \partial y$ and $\partial \bar{v} / \partial x$ are time-averaged velocity gradients (Nezu and Nakagawa, 1993, p. 65). In turbulent flows, the eddy viscosity can be approximated as equal to the mixing coefficient (Rutherford, 1994, pp. 28-31). This method allowed the mixing coefficient to be determined entirely by measured quantities, with all dependence on empirical relations and estimations removed. To get a single value for the mixing coefficient, the eddy viscosity was calculated for each point in the profile and then averaged over the depth.

Empirical formulas from Table 2 were able to be measured by both the ADV and ADCP. Shear velocity appears in all of the empirical formulas and was handled by extrapolating the measured $-\langle u'w' \rangle$ profile to the bed. Geometric quantities required were easily obtained by measuring the flow once it was stable. Measurements from both the ADV and ADCP were used with the empirical formulas and compared with each other and the new method.

CHAPTER 4: RESULTS AND DISCUSSION

Introduction

Data collected from the two cases with different values of H/B are presented in multiple manners. Components used to check the quality of data are presented. This includes a long time record to establish steady state, a pair of turbulence spectra from ADV measurements, and intensity profiles for the ADCP. Flow quantity measurements from the ADCP and ADV are presented and compared. These measurements are grouped into three functional categories: mean velocity profiles, Reynolds stress profiles, and turbulent kinetic energy profiles. The values from each of these categories are then combined with geometric measurements to estimate the transverse mixing coefficient using the new method proposed in chapter 3. Estimates from the proposed method are compared with existing empirical methods presented in chapter 2 and used to assess the ability of ADCPs to accurately estimate the transverse mixing coefficient.

Evaluation of Sampling Conditions

This subsection has three main components – the establishment of steady state with a long ADV record, a turbulence spectrum and ADCP intensity profiles. All of these components were used to check the quality of data collected and help understand nuances specific to this laboratory. ADCP intensity profiles were used to see if a significant difference existed between the two H/B cases tested. These two cases were initially chosen based on geometric recommendations from Teledyne and the capacity of the flume.

A long record was taken with the ADV to test for steady flow in the flume prior to any comparative measurements. Testing for large scale variations can be achieved with a

lower sampling frequency than is required for testing turbulence. Almost instantly values settle into a range within 5% of the long-term average and remain within 1% for the last hour of the test (Figure 8). Flow in the flume was considered steady based on these results. Additionally, this test provided reassurance that a 5 minute sampling time for comparison datasets is sufficiently long.

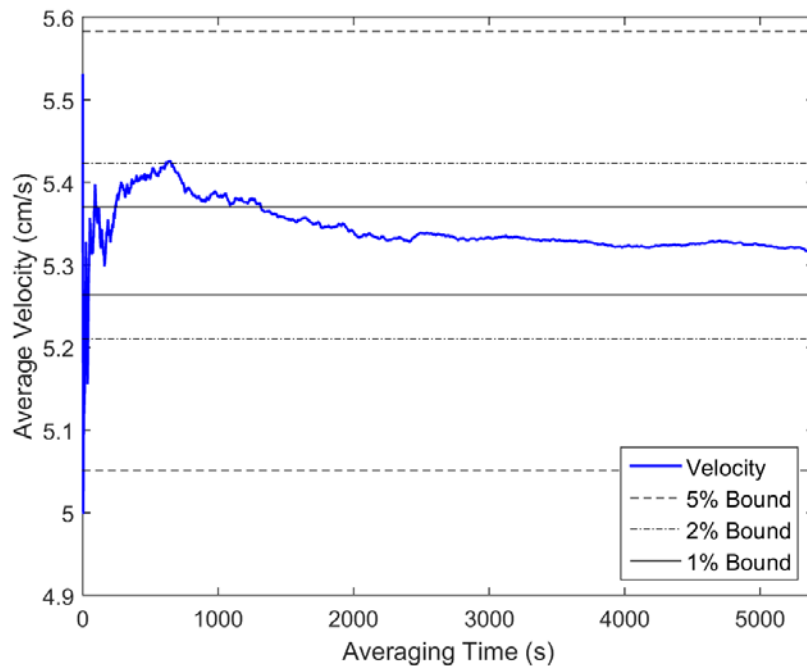


Figure 8 – Cumulative average of streamwise velocity at 9 cm above the bed.

A fairly prominent spike in the ADV turbulence spectrum is observed around 10 Hz for locations close to the bed (Figure 9). During testing, a pronounced vibration could be seen on the water surface. This spike is likely related to those ripples visible on the surface. No solution has been found to completely remove the vibrations at this time. Plotting the spectrum served as a way to identify abnormal frequencies that may be influencing the data. The spike itself is small compared to the rest of the profile, and may be insignificant. Further filtering of noise would help quantify the impact.

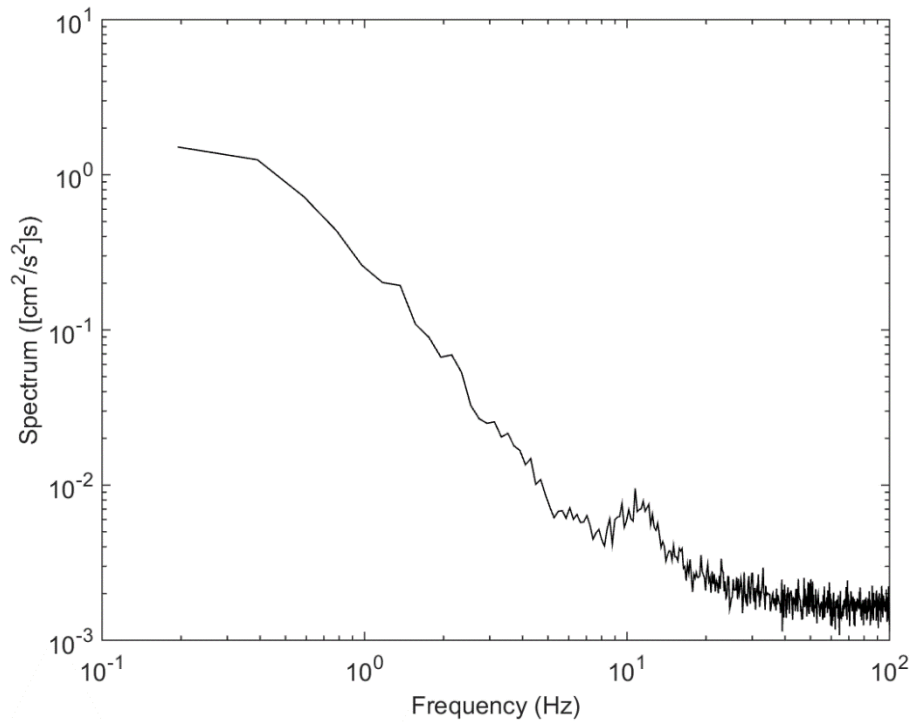


Figure 9 – Averaged frequency spectrum calculated for data collected at $y = 0$ and $z = 5$ cm.

Locations farther from the bed did not exhibit the same spike around 10 Hz (Figure 10). One possible explanation is water flowing into the flume created a vibration that aligned with a resonant frequency of the physical structure. In addition to visible vibrations on the surface, vibrations could be felt by touching the main structural components of the flume. Because the ADV was mounted on a cart attached to the flume, the cart would be subjected to the same vibrations. As the ADV was lowered into the flow, the effective length of the supporting rod increased, thus changing resonant frequency. It is possible that near-bed locations were more sensitive to motion. Movements in the supporting structure will have a small influence on ADV measurements. Because this frequency spike was observed only near the bed, the influence was not considered significant to the entire profile.

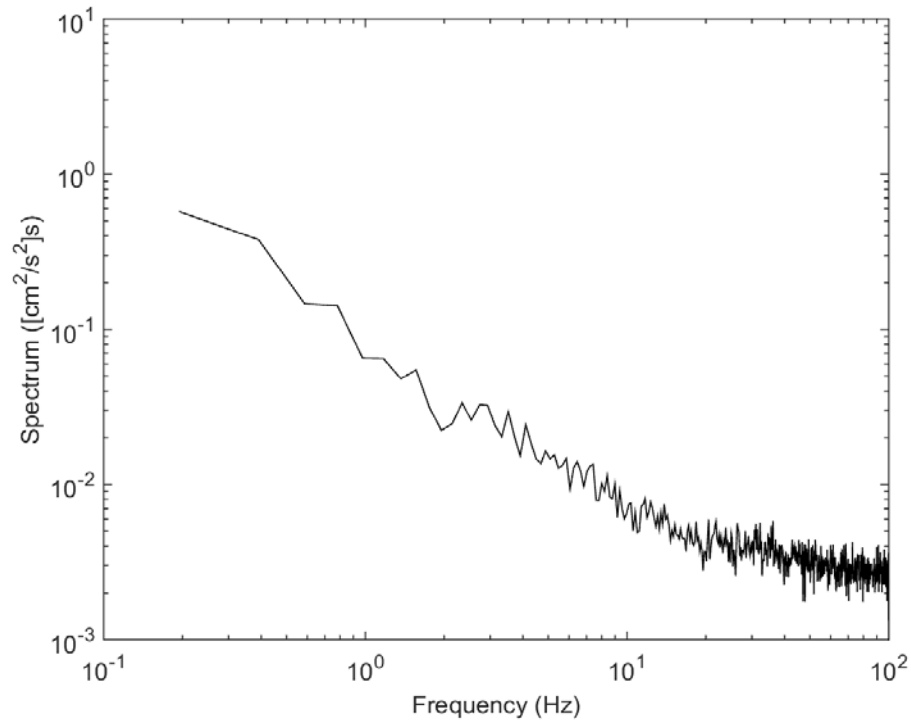


Figure 10 – Averaged frequency spectrum calculated for data collected 5 cm from the bed in the center of the channel

Average intensity profiles for ADCP measurements showed minimal change between the two cases near the surface (Figure 11). It is important to notice the variation in the first case ($H/B = 0.47$) below the region of side-lobe interference. This raises questions on the accuracy of the instrument, especially in depth cells close to the bed. Readings below the bottom of the channel are likely due to reflections from the walls. These reflections take longer to return to the transducer. Since the instrument associates depths with measurements based on return time, the reflected signals would be processed as deeper points. The second case did show signs of a poor signal farther from the bed, although the phantom points below the surface were missing. Poor intensity near the bed is likely related to the larger H/B ratio and the beams spreading into the walls before

reaching the bottom of the channel. Testing the ADCP in a wider channel would help identify the impact of narrow and reflective sidewalls.

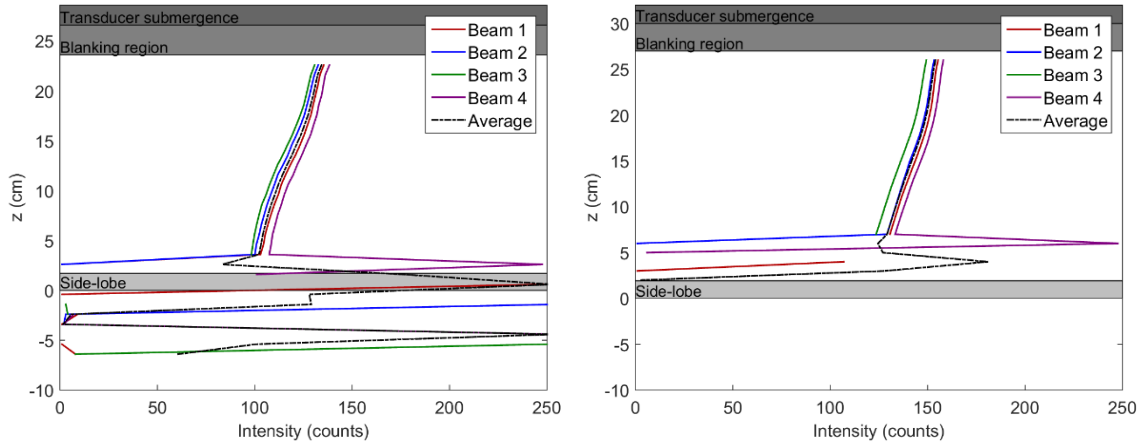


Figure 11 - ADCP intensity profiles for $H/B = 0.47$ (left) and $H/B = 0.53$ (right)

Comparison of Mean Velocity

ADCP streamwise velocity values are consistently lower than those from the ADV (Figure 12). Closer to the bed, the difference is less apparent. The agreement between the two beam pairs is promising, and can be used to highlight a mechanism behind the underestimation. Because the beams are oriented 45° off streamwise, the velocities are measured at locations offset from the middle. Closer to the walls and farther from the center velocities will drop. Measurements at both the surface and bed were not obtained due to the transducer being submerged, manufacturer specified blanking distance, and the area of side-lobe interference. These regions of no measurement are shown as shaded areas in each plot.

The streamwise mean velocity profile for $H/B = 0.53$ (referred to as the second case) shows more agreement than $H/B = 0.47$ (referred to as the first case). Creating a smaller ratio also created a faster flow. A faster flow will register with the ADCP in a central measuring region whereas the slower flow associated with $H/B = 0.47$ will start pushing

the boundaries of slow flows the instrument can detect. An area of flow directly above the area of side-lobe interference was not measured for $H/B = 0.47$. These bins were marked “BAD” in WinRiverII, and flagged in the output file based on poor correlation values.

Near-surface measurements from the ADCP curve decrease at a faster rate than ADV measurements, a characteristic also noted in the profiles obtained by Nystrom et al. (2007). The difference in velocity profiles here is exaggerated partly by the scale on which velocities were recorded and by the beam orientation. For the profiles shown in Nystrom et al. (2007), the velocities measured were 2-3 times larger than those measured in these profiles. The ADCPs used in this work and the work of Nystrom et al. (2007) have the same absolute degree of accuracy. The impact of this accuracy on the two flows is distinctly different. For example, if the ADCP is capable of measuring flow to the nearest 0.2 cm/s, the potential error related to a flow with a maximum velocity of 6 cm is much greater than the error associated with a velocity of 20 cm.

A second component behind the exaggeration of differences can be traced back to the beam orientations used. For these tests, the beams were oriented 45° off streamwise, which caused velocities to be measured just off the centerline of the channel and away from the location the ADV was measuring. In the work of Nystrom et al. (2007), the beams were oriented with two beams perpendicular to and two beams parallel with the streamwise streamline. This orientation allowed velocities to be measured directly in line with the ADV, leading to more accurate results.

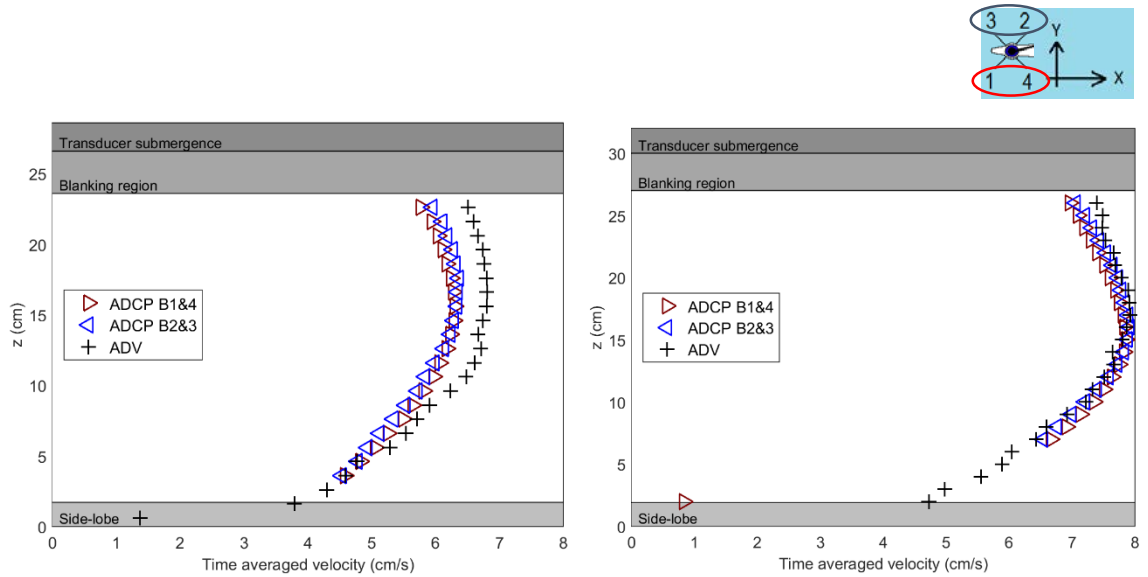


Figure 12 – Streamwise velocity profiles obtained by ADV and ADCP for $H/B = 0.47$ (left) and $H/B = 0.53$ (right). Beam pairs used in calculations shown top right.

Transverse velocities show visible differences between instruments (Figure 13). The ADV measured profile varies from zero, which is qualitatively in line with vector descriptions in Nezu and Nakagawa (1993, p. 101). Velocity magnitudes for ADV measurements look similar in magnitude to the vector descriptions. ADCP values, however, are significantly larger in magnitude than both ADV measurements and the Nezu and Nakagawa descriptions. More pronounced in the second case measurements is the change in sign between ADV and ADCP profiles. The transverse direction contained the most freedom of movement of any direction. This freedom, while very small, may have impacted the collected profiles.

Stacey et al. (1999) found that motion in the boat an ADCP is mounted on can set a level of bias in collected datasets. They found vertical motion as the most difficult to account for based on measurable pitch and roll quantities. Bottom tracking was disabled for these tests. Without information on transverse and streamwise translation that is

acquired through bottom tracking, the instrument is not be able to make corrections for drift automatically, which could potentially bias data. Creating an environment where bottom tracking can be enabled without reducing the quality of velocity data may show improvement as the ADCP can better account for motion.

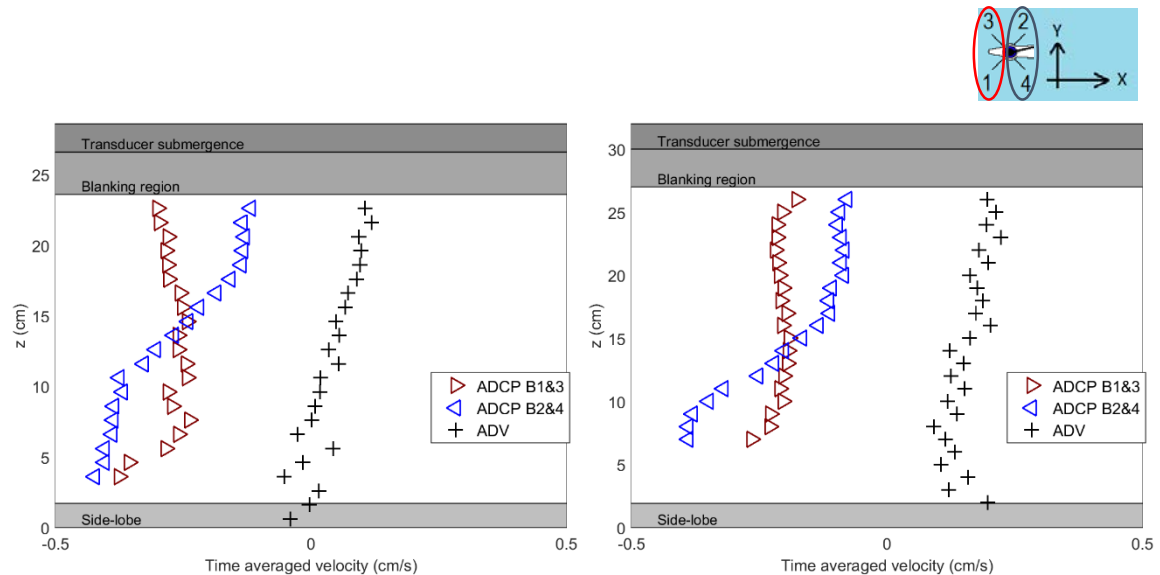


Figure 13 – Vertical profiles of transverse velocity obtained by ADV and ADCP for $H/B = 0.47$ (left) and $H/B = 0.53$ (right). Beam pairs used in calculations shown top right.

The vertical velocity profile shows limited agreement between the ADCP and ADV profiles, mostly in the lower portion of the flow for both cases (Figure 14). Vertical velocity profiles, mostly in the lower portion of the flow for both cases (Figure 14). Vertical velocity magnitudes are expected to be much less than streamwise components (Nezu and Nakagawa, 1993, p. 101), making the limited agreements more impressive. Unlike the streamwise component, vertical velocities are larger in magnitude than their ADV counterparts. Extracting the vertical velocity component requires combinations of either beams 1 and 2 or beams 3 and 4. This averaging scheme places the average velocity value in the center of the transducer, whereas the streamwise and transverse velocities are placing averages on either side of the centerline or in front or behind the transducer. The lone near-

bed velocity point appears again on this profile, with only one pair of beams registering a physical real number.

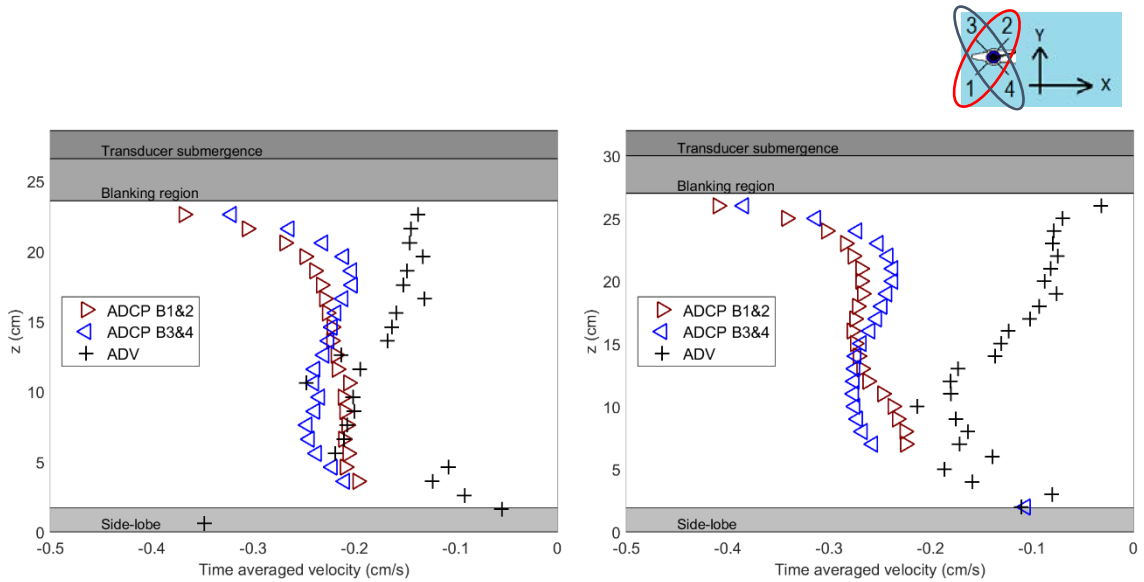


Figure 14 - Vertical profiles of vertical velocity obtained by ADV and ADCP for $H/B = 0.47$ (left) and $H/B = 0.53$ (right). Beam pairs used in calculations shown top right.

Overall, the second case returned results better than expected for the mean velocity profiles. The maximum recommended H/B ratio for testing in laboratory settings is 0.5 (Teledyne, personal communication). In channels with a larger ratio, concerns about acoustic reflections become relevant. The difference in ratios for these two cases is very small, and could not be easily expanded due to facility limitations. Expanding the extremes would help better map where the ADCP's ability to accurately measure velocity breaks down.

The biggest difference between the two cases was the appearance of a near-bed point in the second case profiles. For each of the cases the streamwise profiles had the most agreement in velocity magnitude. The same general shape was observed between the flows, highlighting a consistent flow pattern in the flume. Vertical velocities showed limited

agreement, while transverse velocities were equally poor between cases, with the magnitude being much larger for ADCP measurements than the ADV recorded. Variation between ADCP and ADV measurements for all three components for each case may be linked to the geometric locations velocities were averaged in. Vertical velocities were averaged over the center of the transducer, and they were closer in terms of absolute difference than streamwise or transverse velocity, with all three directions showing the best agreement near the middle of the flow (Figure 15). Streamwise velocities were averaged over points offset from the centerline of the channel, and as such should experience different velocities. Likewise, vertical velocities averaged at points upstream and downstream of the transducer and likely experienced different velocities.

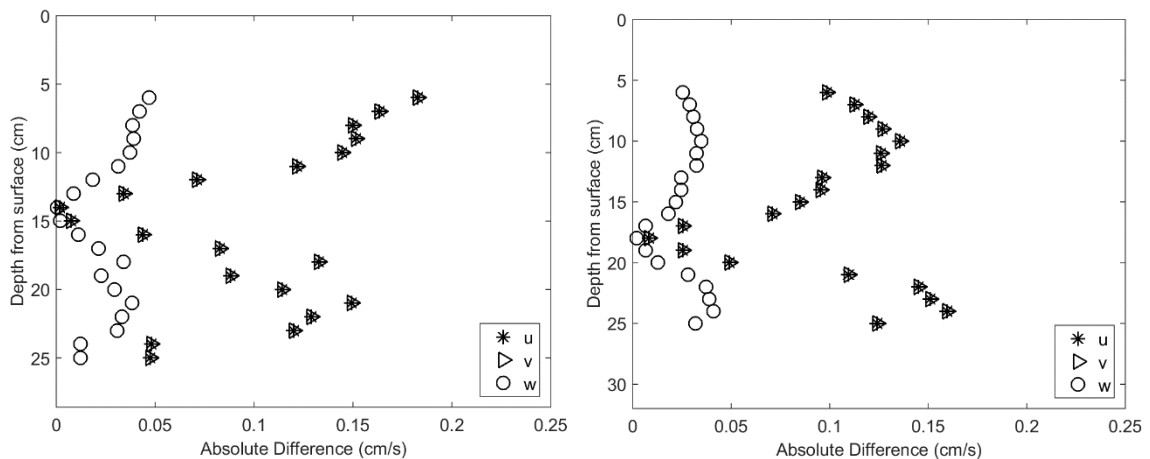


Figure 15 - Absolute difference in beam velocity pairs for $H/B = 0.47$ (left) and $H/B = 0.53$ (right)

Comparison of Reynolds Stresses and Turbulent Kinetic Energy

Each of the six Reynolds stress component profiles were calculated for data from the ADV and ADCP for each of the two values of H/B . The results are presented in two groups of three. The Reynolds shear stresses are presented as the first group and the Reynolds normal

stresses, or mean-squared velocity fluctuations, are presented second. Overall, these groupings showed similar trends for each value of H/B . The Reynolds shear stress profiles matched well for both groups. However, the Reynolds normal stresses did not exhibit as much agreement for either of the two cases measured.

In a fully developed flow, the $-\langle u'w' \rangle$ component is expected to be near linear, ranging from the maximum value at the bed to zero at the surface (Joung and Choi, 2010). This linear trend appears near the channel bottom for both cases. The remaining shear stresses, $-\langle u'v' \rangle$ and $-\langle v'w' \rangle$, are expected to be near zero on the centerline of the channel, with a slight deviation near the bed and surface based on direct numerical simulations done by Joung and Choi (2010). The normal stresses all show gradients that increase closer to the bed.

The $-\langle v'w' \rangle$ and $-\langle u'w' \rangle$ shear stresses appear to reproduce well between instruments for both cases (Figure 16). A larger range of values was observed for the second case in the $-\langle u'v' \rangle$ and $-\langle v'w' \rangle$ profiles, especially in the lower region of flow. For both cases, the $-\langle u'v' \rangle$ profile appeared more scattered for both instruments making it hard to identify a coherent profile. Measuring profiles for $-\langle u'v' \rangle$ and $-\langle v'w' \rangle$ with respect to the transverse direction may provide a more distinctive profile shape that matches the simulations done by Joung and Choi (2010).

The results from these tests show what appears to be a larger percent error in $-\langle u'w' \rangle$ profiles compared to results from Nystrom et al. (2007). It is important to note that Nystrom et al. were able to test in deeper flow and achieve higher maximum Reynolds shear stress values. The error between values here may be impacted significantly by the low flow and generally smaller stresses obtained.

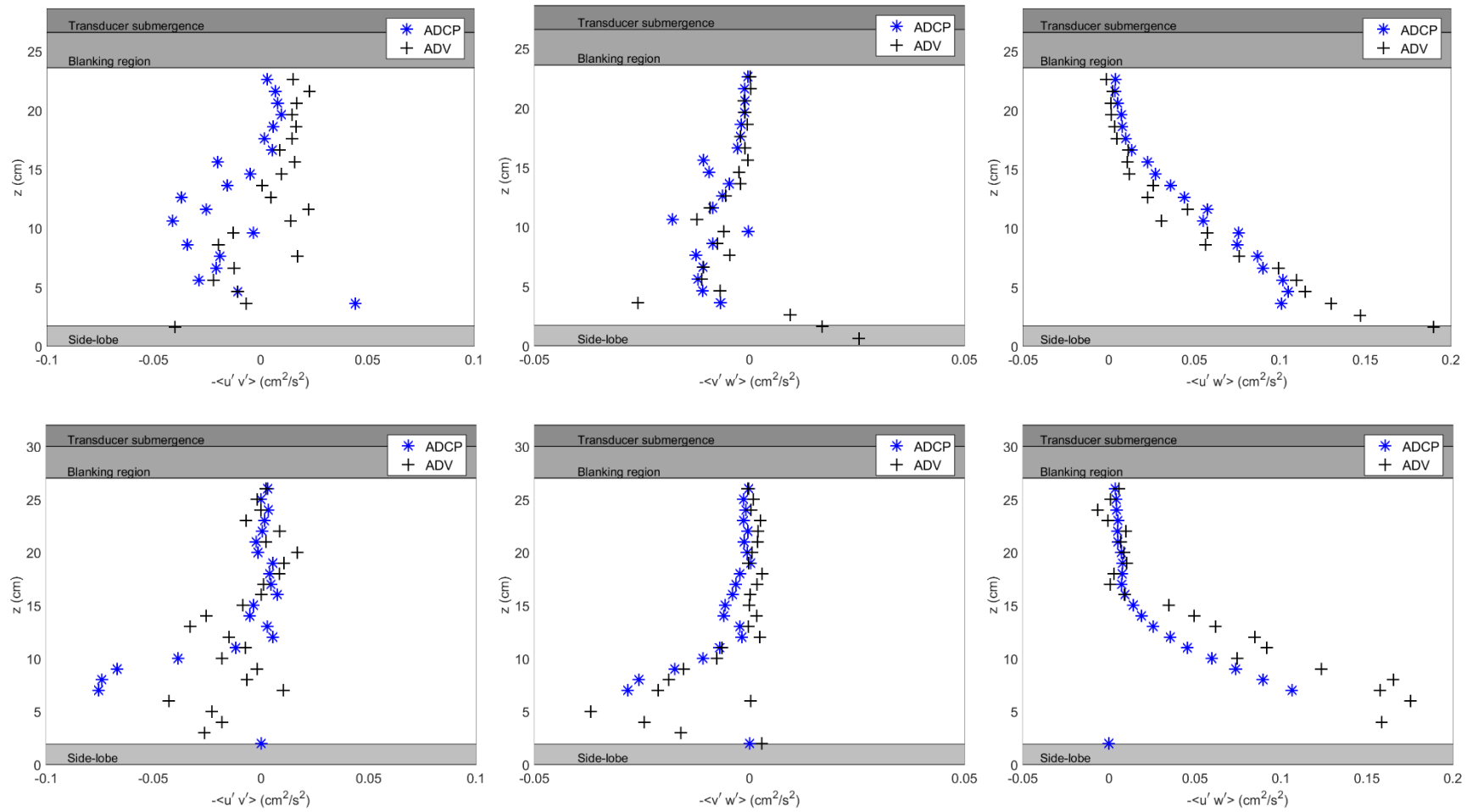


Figure 16 – ADV and ADCP measured Reynolds shear stress profiles for $H/B = 0.47$: $-\langle u'v' \rangle$ (top left); $-\langle v'w' \rangle$ (top center); $-\langle u'w' \rangle$ (top right); and $H/B = 0.53$: $-\langle u'v' \rangle$ (bottom left); $-\langle v'w' \rangle$ (bottom center); $-\langle u'w' \rangle$ (bottom right).

The vertical normal stress was the most impressive, showing agreement throughout the profile between instruments for both cases (Figure 16). ADCP streamwise and transverse normal stresses were consistently low but did capture the shape of ADV measurements well. Results from Voulgaris and Trowbridge (1998) indicate that the ADV has difficulty measuring the streamwise and transverse stresses. A scatter exists in the ADV profiles which is especially evident in the transverse normal stress. Noise has larger effect on the streamwise and transverse stresses, which likely contributes to this scatter. If noise is increasing ADV measurements, it becomes more difficult to assess the accuracy of the ADCP. The smoothness of ADCP profiles hints at two different items – either the ADV mounting system is introducing extra noise as previously discussed or the ADCP may not be accurately measuring and computing fluctuations. Running a test with the ADV mounted on an external frame may help identify if the mount is a prominent source of noise. Running a test that includes a wider and deeper flow would move values into a central measuring region for the ADCP, potentially helping to eliminate errors.

Generally the error between normal stresses measured between instruments is much better than the errors seen between shear stresses (Figure 18). The qualitative difference between cases for the shear stresses is intriguing. Error in $-\langle u'v' \rangle$ becomes smaller for the second case while error in the $-\langle v'w' \rangle$ case increases. Both components rely on transverse velocities, which was the most irregular of the three directions. These changes and increased error may be due to the connection with the transverse direction. Errors for the normal stresses showed less variation between cases, especially with regard to the transverse direction.

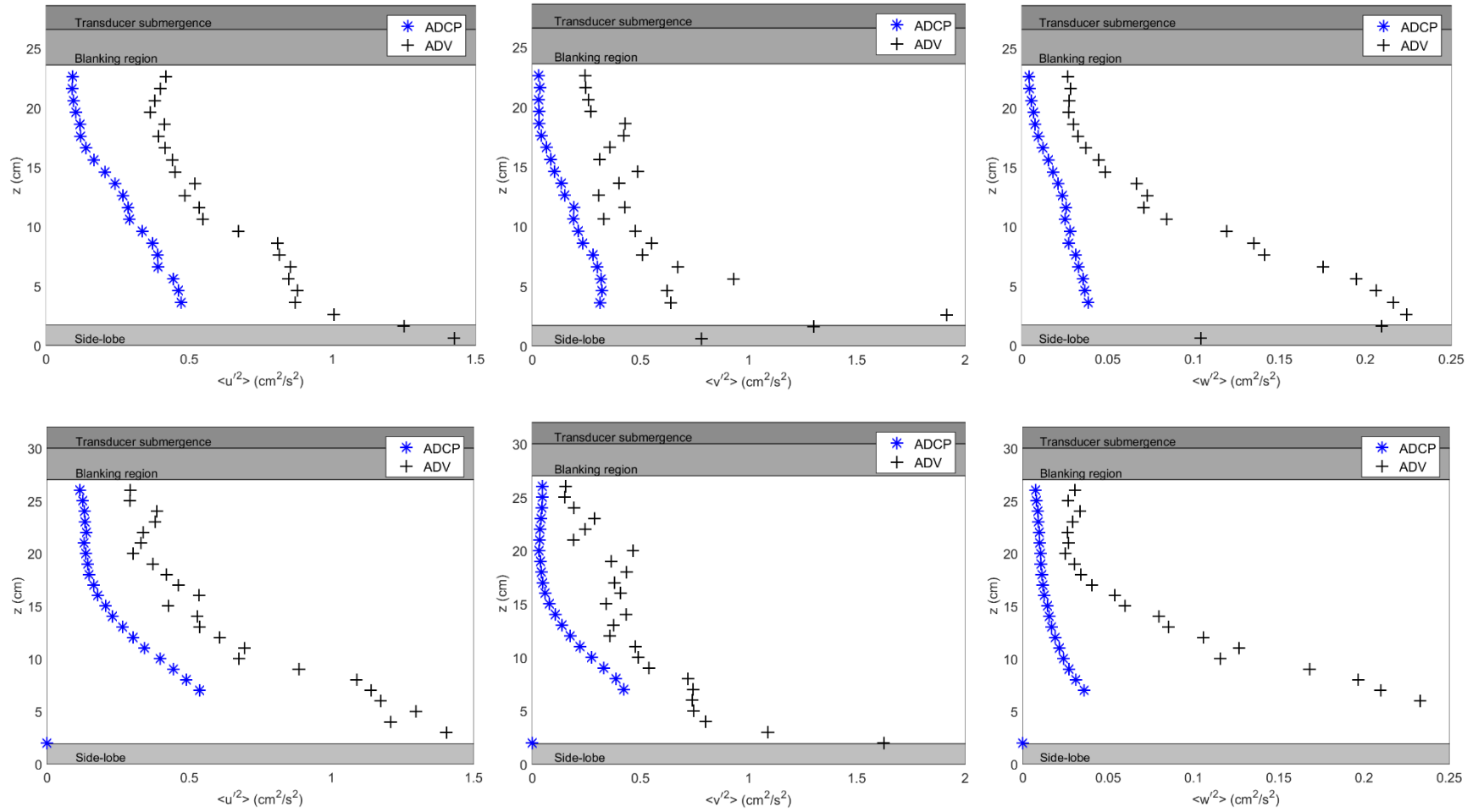


Figure 17 - ADV and ADCP measured Reynolds normal stress profiles for $H/B = 0.47$: $-\langle u'^2 \rangle$ (top left); $-\langle v'^2 \rangle$ (top center); $-\langle w'^2 \rangle$ (top right); and $H/B = 0.53$: $\langle u'^2 \rangle$ (bottom left); $\langle v'^2 \rangle$ (bottom center); $\langle w'^2 \rangle$ (bottom right).

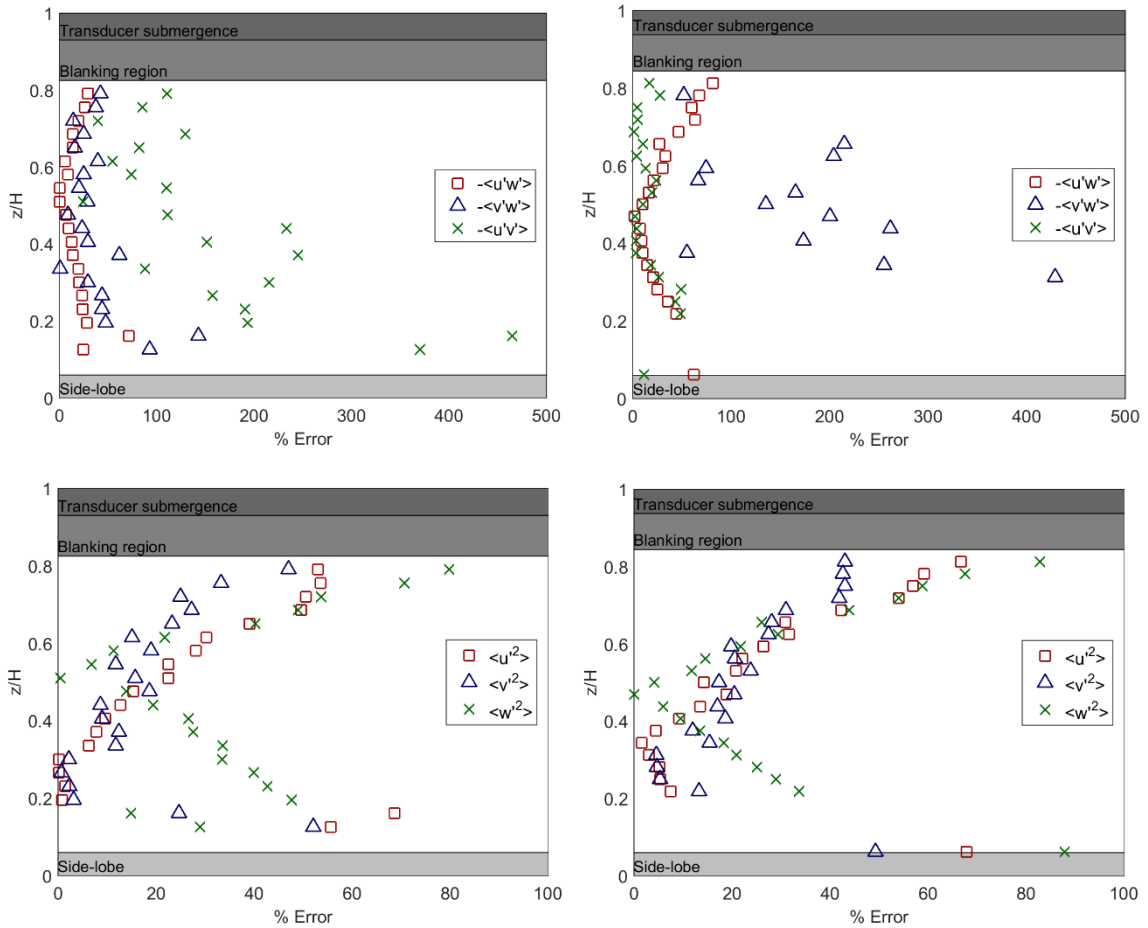


Figure 18 – Percent error in Reynolds shear stresses for $H/B = 0.47$ (top left) and $H/B = 0.53$ (top right); Percent error in Reynolds normal stresses for $H/B = 0.47$ (bottom left) and $H/B = 0.53$ (bottom right)

As shown in Chapter 3, each of the six Reynolds stresses can be calculated two different ways. The beams are not sampling the same volume, so fluctuations resulting from cross-beam correlations are unknown. However, the beam correlation averages are assumed to be the same with the assumption of statistical homogeneity. This renders the equations that use beam correlations typically more accurate than the equations that use cross-beam correlations (Figures 19 and 20). Obvious differences appear towards the bottom of the profile due to increasing distance between beams. Beams sampling farther apart will experience different conditions making homogeneity assumptions less valid.

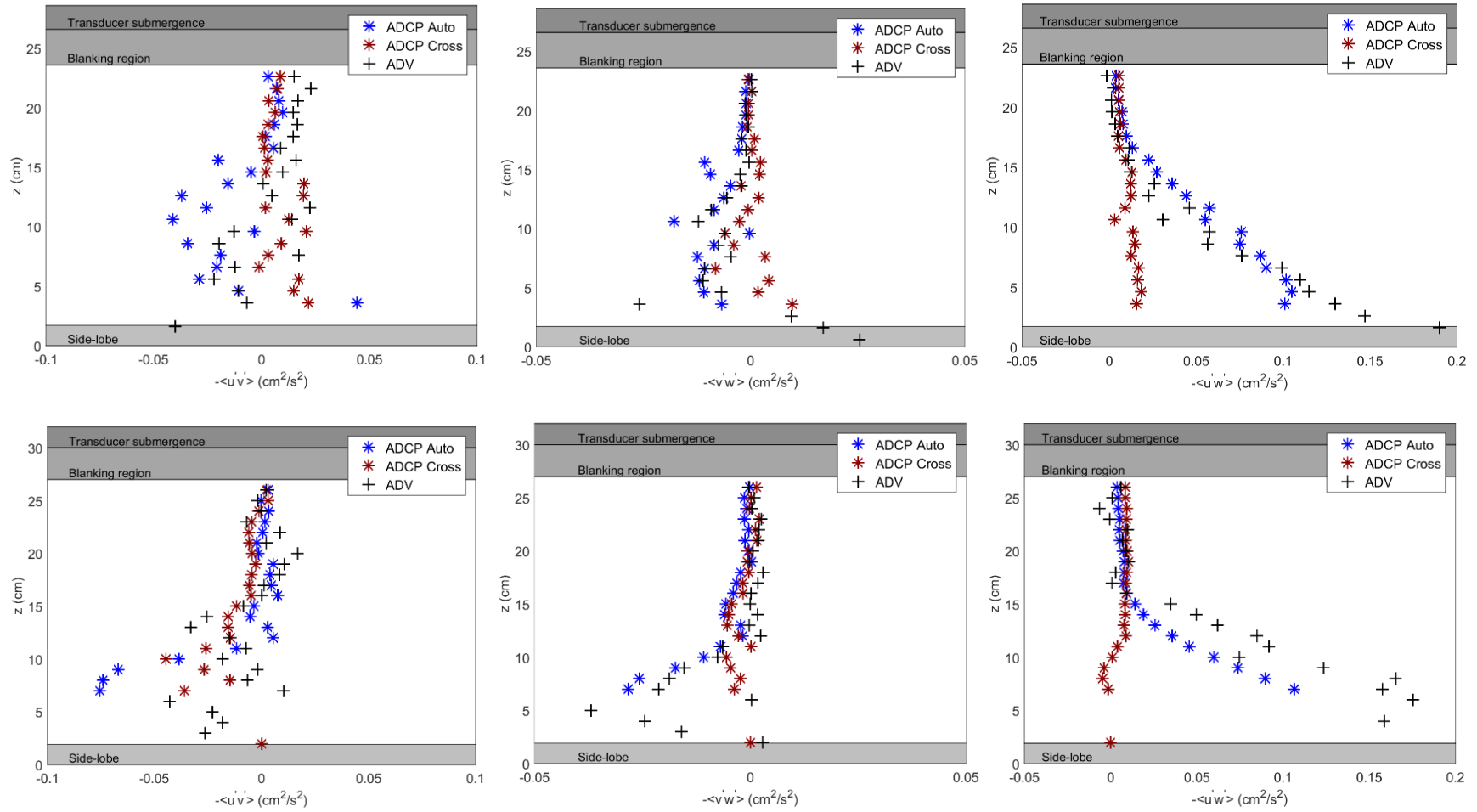


Figure 19 - ADV and ADCP measured Reynolds shear stress profiles calculated two ways for $H/B = 0.47$: $-\langle u'v' \rangle$ (top left); $-\langle v'w' \rangle$ (top center); $-\langle u'w' \rangle$ (top right); and $H/B = 0.53$: $-\langle u'v' \rangle$ (bottom left); $-\langle v'w' \rangle$ (bottom center); $-\langle u'w' \rangle$ (bottom right).

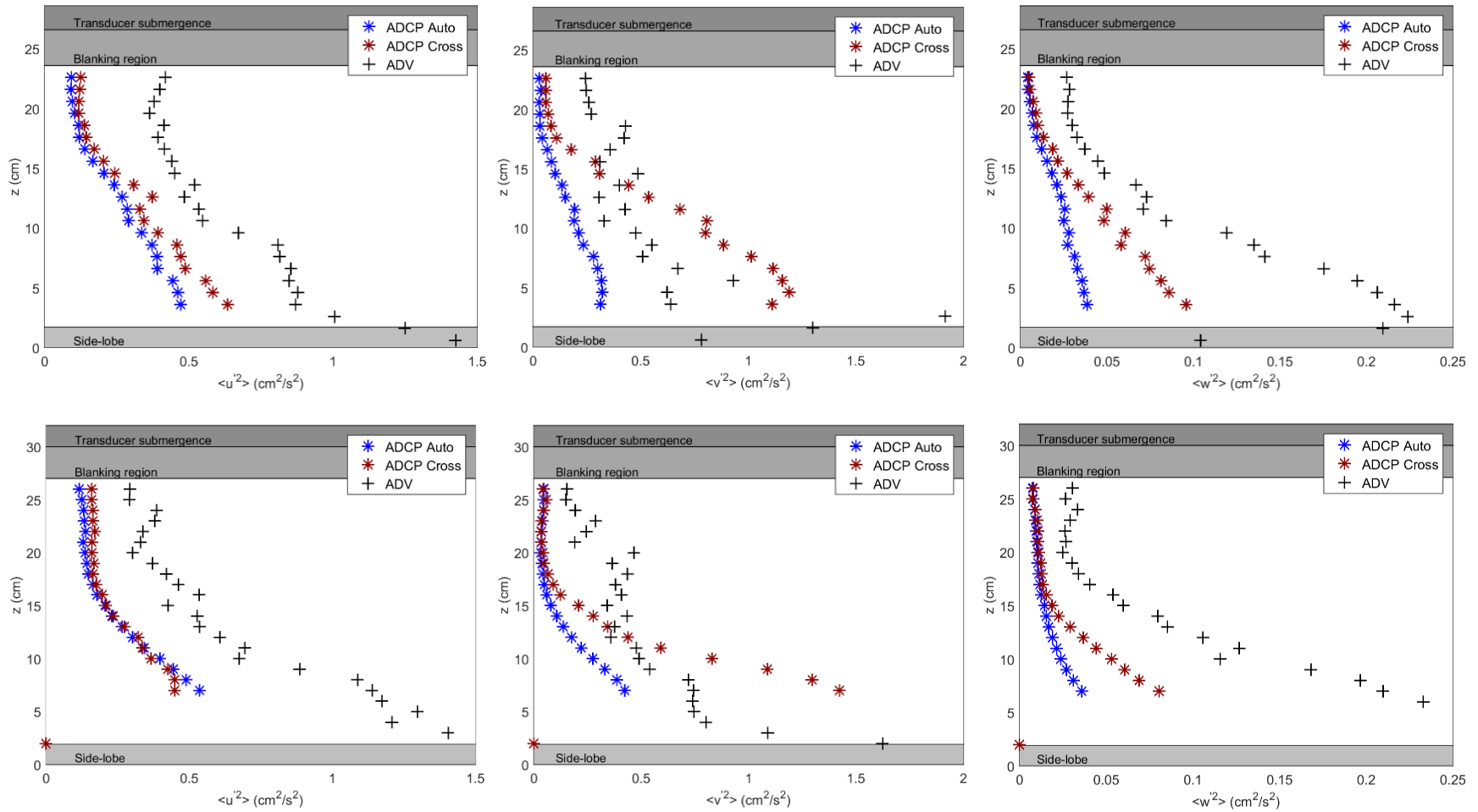


Figure 20 - ADV and ADCP measured Reynolds normal stress profiles calculated two ways for $H/B = 0.47$: $-\langle u^2 \rangle$ (top left); $-\langle v^2 \rangle$ (top center); $-\langle w^2 \rangle$ (top right); and $H/B = 0.53$: $-\langle u^2 \rangle$ (bottom left); $-\langle v^2 \rangle$ (bottom center); $-\langle w^2 \rangle$ (bottom right).

Not surprisingly, ADCP measurements of turbulent kinetic energy (TKE) are consistently low compared to ADV values for each of the two cases measured (Figure 21). Two of the three measured components used in calculating TKE consistently had the ADCP lower than the ADV, with the third component matching better. With low estimates as inputs, a low estimate as an output makes sense. Further analysis to remove possible noise from ADV measurements will aid in determining if the ADCP is in fact low or if the ADV is overestimating fluctuations by including noise.

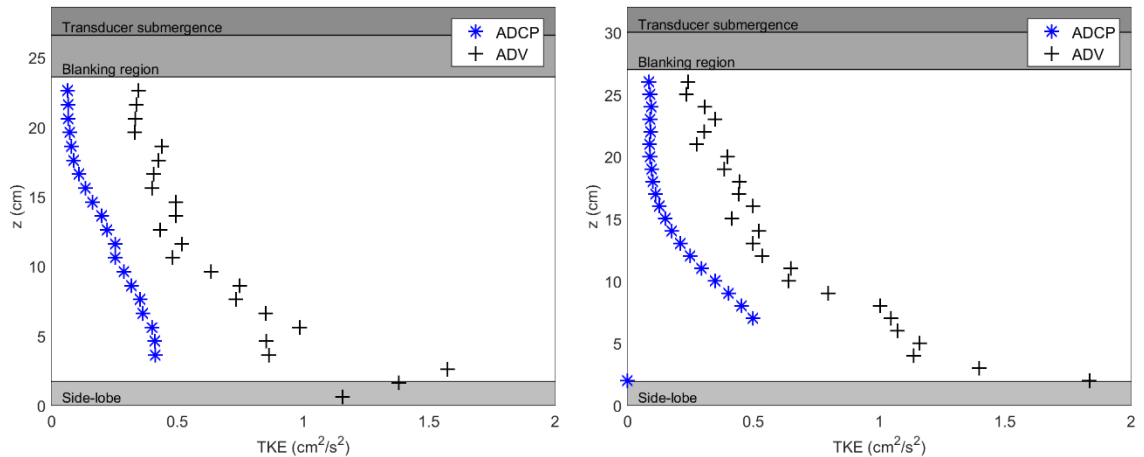


Figure 21 - TKE profiles for H/B of 0.47 (left) and 0.53 (right).

Transverse Mixing Coefficient Estimates

The proposed method using ADCP measurements to estimate transverse mixing produces similar values as at least one empirical formulas for one of the two cases tested (Figure 22). The proposed method shows the most agreement with the estimate of Fischer et al. (1979), an estimate which was determined using a straight channel in a laboratory. This setting matches the setting in which data were collected and makes the consistency across empirical estimates using ADV data, empirical estimates using ADCP data and proposed methods impressive.

Less agreement would be expected between the proposed method and the empirical methods of Bansal (1971), Deng et al. (2001), and Jeon et al (2007). These formulae were based on field measurements. In the field, typical conditions are much different from those encountered in a controlled environment. Rivers are not perfectly straight, nor do they have a consistently uniform bed. In the case of Deng et al. (2001), the empirical estimate includes a component based on secondary currents. Other mechanisms of dispersion become more important in larger rivers, and as the test channel was small compared to many natural channels, these other mechanisms can be considered insignificant.

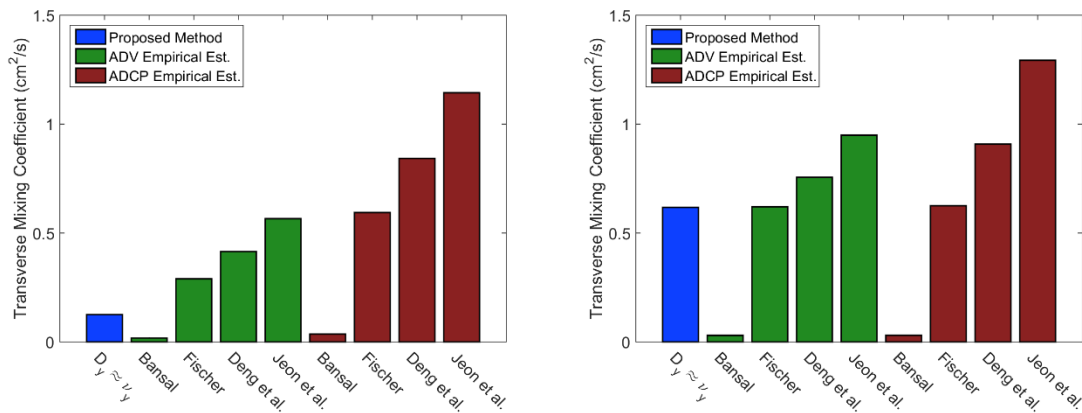


Figure 22 - Transverse mixing coefficient estimates for flume flow for $H/B = 0.47$ (left) and $H/B = 0.53$ (right)

The proposed method does not compare as well with empirical estimates for the $H/B = 0.47$ case. Agreement between the ADCP and ADV empirical estimates is worse for this case as well. For $H/B = 0.53$, the empirical estimates between instruments show reasonable agreement, with Fischer's estimate standing out as excellent. The estimates based on field data show more variance, but not as much as the $H/B = 0.47$ case. The Jeon et al. estimate is off by a factor of 2 between instruments for $H/B = 0.47$ while the estimate is off by less than 1.5 times for $H/B = 0.53$. For Deng et al., Fischer and Bansal this gap between factors increases. Estimating within a factor of 2 in transverse mixing is

considered good, especially when empirical estimates span an order of magnitude or more (Figure 1).

In the shallower, slow flow, the smaller velocity magnitude may have impacted the ability of the ADCP to accurately capture fluctuations. The smallest fluctuations and velocities may have been smaller in magnitude than the minimum resolution of the ADCP and may not have recorded accurately. The two smallest quantities used in calculating transverse mixing coefficient are $-\langle u'v' \rangle$ and the transverse velocities. Transverse velocity magnitudes measured by the ADCP were large compared to ADV measurements, which would drive the transverse mixing coefficient calculation down. Likewise, $-\langle u'v' \rangle$ estimates from the ADCP tended to be low compared to the ADV, which also drives down the transverse mixing coefficient. In a faster flow, these differences are likely less apparent, and would contribute less error to the proposed method for calculating transverse mixing. The agreement between empirical transverse mixing estimates and the proposed method in the second case is encouraging and provides evidence that this method is worth exploring further by testing against tracer studies.

CHAPTER 5: CONCLUSIONS

Summary

Accurate estimates for transverse mixing are important in estimating dispersion in channels. One mechanism for measuring dispersion is the theory of shear dispersion. Geometric variables are combined with velocity profiles in this theory to calculate dispersion. The transverse mixing coefficient is used as well, but is typically estimated using one, or more, of a number of empirical formulas. These formulas span a wide range and provide inconsistent results. Measuring dispersion with ADCPs has been investigated by previous researchers with promising results. However, measurement and handling of the transverse mixing coefficient has not been standardized or addressed in detail. A method was proposed to estimate transverse mixing based on the ability of ADCPs to measure turbulence.

Results from two cases were analyzed to assess the ability of ADCPs to measure turbulence. Quality of measurement parameters were inspected to understand the flow and identify potential problematic areas. Results from a stationarity test revealed that the flume was able to maintain a steady flow for the time required to complete a measurement. Though not the primary purpose, these tests were also able to provide reassurance that the testing duration was long enough. Frequency spectra from a pair of ADV comparison measurements were examined in detail and they showed the presence of a frequency spike in measurements near the bed. Farther from the bed this frequency spike is not present, indicating that it likely does not have a significant effect on the flow. To gain a better sense of the quality of ADCP data, average intensity profiles were inspected for each case. The first case showed signs of excess acoustic reflection resulting in phantom bins below the

bed. These phantom bins did not record any velocity and they had little effect on profile calculations. The second case showed signs of reflection in the main zone of measurement, which may have had a small impact on the data quality near the bed. Both cases showed strong intensity in the upper region of flow, indicating good signal quality and a high confidence in the data collected.

Mean velocity profiles for the two cases matched well overall. Values from the ADCP were typically less than those measured by the ADV in the streamwise direction. Low values were attributed to the alignment of the beams and the geometry required to compute the mean velocity. Results from Nystrom et al. (2007) showed better agreement between instruments, but the beam alignment was different, with beams oriented parallel and perpendicular to the streamwise direction. That alignment would produce results measured directly in the center of the channel, improving the chance for accurate measurement and comparison. The same qualitative shape was observed between results measured by Nystrom et al. (2007) and for each of the two cases measured here. A prominent consistent feature was the reduction in velocity near the ADCP transducer. This reduction in velocity was also seen in ADV measurements. Measurements for each of the two cases did not record any data for bins within the recommended blanking distance whereas the Nystrom et al. (2007) dataset included some bins within that space. However, the blanking distance for the ADCP used here is much smaller than four-beam ADCP used previously.

Transverse velocities did not match well between instruments, with the ADCP for both cases measuring velocities off by both sign and magnitude. ADV values matched well qualitatively with the values expected by Nezu and Nakagawa (1993, p. 101). Vertical

velocities showed much better agreement than transverse velocities. Agreement between beams was good. Similarly to the streamwise velocity profile, vertical velocity showed a bending in the profile near the transducer.

Reynolds shear stress profiles matched well for both cases. ADCP estimates had a tendency to be less than ADV values. Noise in ADV measurements may be falsely inflating values, reducing the difference between the two instruments. The $-\langle u'w' \rangle$ component looks initially to be worse than the results reported by Nystrom et al. (2007). However, the scale on which $-\langle u'w' \rangle$ was reported is almost 10 times that measured in this study. A percent error at each specific depth would provide a better insight into which study produced better agreement between instruments. The Reynolds normal stresses measured by the ADCP were also consistently lower than the results measured by the ADV. Again, noise in the ADV measurements may be falsely increasing values, leading to worse agreement. Qualitatively the measurements agreed.

The proposed method for measuring the transverse mixing coefficient with ADCP values aligned well with empirical estimates for the second case. Fischer's estimate for transverse mixing, developed using data from a straight laboratory channel, provided the best agreement. Other formulas based on field data were larger, but likely include effects beyond simply turbulence that contribute to transverse mixing. The proposed method did not match as well for the first case. The limited velocity scale at that flow may have impacted the ability of the ADCP to accurately catch fluctuations and ultimately compute the transverse mixing coefficient. The second case is promising, and it provides reason to continue testing and estimating transverse mixing with ADCPs.

Recommendations and Future Work

Estimates of mean velocities between the ADV and ADCP showed a range of agreement. Testing the ADCP in a wider, faster flow would help determine if the low flows tested here were influenced by technical limitations, such as minimum detectable velocity. The development of an external mounting system for the ADV has the potential to clean up noise and influence the instrument was subjected to from the flume during testing. Performing these tests would help determine if the ADCP was measuring results different than the ADV due to flow conditions, if the ADV was reporting biased data due to external vibrations or if both instruments were sensing values far from the truth.

The proposed method for estimating transverse mixing with ADCPs showed promise based on comparisons with empirical estimates. Not surprisingly, the formula derived using laboratory data in a straight channel matched the best, with formulas derived from field data showing more disagreement. Running similar tests in the field with the ADCP would provide a set of data that can be more realistically compared to these estimates. Additionally dye studies in the field would provide a third method for comparing results. Comparing results with those solely from empirical methods does not necessarily prove that the proposed method is any better than empirical methods. Comparing to data from dye studies would provide a better sense of how accurate the proposed method is and how much improvement is offered over accepted empirical solutions.

APPENDIX A: IMPORTANCE OF VERTICAL VARIATIONS OF VELOCITY FOR SHEAR DISPERSION IN RIVERS

Modified from a paper published in the *Journal of Hydraulic Engineering*, volume 141, issue 10.

Importance of Vertical Variations of Velocity for Shear Dispersion in Rivers

Lauren E. Schwab¹ and Chris R. Rehmann, A.M.ASCE²

Abstract: An expression for the dispersion coefficient in a rectangular channel is derived to evaluate the importance of transverse and vertical variations in velocity for dispersion. The contribution of vertical variations to dispersion depends not on the ratio of the width B and depth H of the channel—as is usually assumed—but on the ratio of mixing times, $\tau = (H^2/D_z)/(B^2/D_y)$, where D_y and D_z are the transverse and vertical mixing coefficients, respectively. The analysis allows the role of vertical variations to be assessed quantitatively as a function of the time scale ratio and the shape of the velocity profile. The time scale ratio is estimated using data sets compiled by others and several empirical formulas for D_y . In almost all cases, vertical variations contribute a small amount to the overall dispersion. The results support the usual practice of considering only transverse variations in computing the dispersion coefficient, and the analysis provides an approach for including vertical variations in calculations of dispersion in cases in which τ is not small.

¹Graduate Research Assistant, Dept. of Civil, Construction, and Environmental Engineering, Iowa State University, Ames, IA 50011.

²Associate Professor, Dept. of Civil, Construction, and Environmental Engineering, Iowa State University, Ames, IA 50011.

Introduction

Shear dispersion is one important mechanism of longitudinal transport of contaminants in rivers. As fluid parcels travel across the cross section in a turbulent flow, they experience larger velocities near the center of the channel and smaller velocities near the banks and bottom. After enough time, the differences in velocities of fluid parcels cause the contaminant cloud to spread diffusively (Fischer et al., 1979, pp. 80-82). Quantitative analysis of this process starts with the governing equation for the contaminant's concentration C :

$$\frac{\partial C}{\partial t} + u \frac{\partial C}{\partial x} = \frac{\partial}{\partial x} \left(D_x \frac{\partial C}{\partial x} \right) + \frac{\partial}{\partial y} \left(D_y \frac{\partial C}{\partial y} \right) + \frac{\partial}{\partial z} \left(D_z \frac{\partial C}{\partial z} \right) \quad (29)$$

where t is time; u is the streamwise velocity; x , y , and z are the streamwise, transverse, and vertical coordinates; and D_x , D_y , and D_z are the mixing coefficients in the three directions. Extending the analysis of Taylor (1953), Fischer et al. (1979, pp. 82-87, 129-130) considered deviations from average velocities and concentrations and simplified (1) using assumptions similar to those in the next section. When transverse variations control the spreading, the longitudinal dispersion coefficient K_T can be computed as

$$K_T = -\frac{1}{A} \int_0^B \hat{u}(y) h(y) \int_0^y \frac{1}{D_y h(y_1)} \int_0^{y_1} \hat{u}(y_2) h(y_2) dy_2 dy_1 dy \quad (30)$$

where A is the area of the cross section, B is the top width of the channel, $h(y)$ is the depth at transverse position y , and \hat{u} is the deviation—averaged over the depth—from the mean velocity \bar{u} for the cross section. In a similar way, if only vertical variations control the spreading, the longitudinal dispersion coefficient K_V can be computed as

$$K_V = -\frac{1}{A} \int_0^H \tilde{u}(z)b(z) \int_0^z \frac{1}{D_z b(z_1)} \int_0^{z_1} \tilde{u}(z_2)b(z_2) dz_2 dz_1 dz \quad (31)$$

where H is the maximum depth, b is the width at vertical position z , and \tilde{u} is the deviation—averaged over the transverse direction—from \bar{u} .

Equations (2) and (3) have been used to develop formulas for the dispersion coefficient and compute the dispersion coefficient directly from velocity measurements. Elder (1959) used (3) to compute the dispersion coefficient based on logarithmic vertical variation of the velocity. Fischer et al. (1979, p. 136) used (2) and estimates of the integrals from field measurements to develop a formula for the dispersion coefficient, while Deng et al. (2001) used approximate analytical expressions for the velocity and channel geometry to develop another empirical formula. Fischer (1967) computed the dispersion coefficient directly from point measurements of the velocity in the Green-Duwamish River. Carr and Rehmann (2007) showed that the dispersion coefficient computed from (2) and the more detailed velocity fields produced by an acoustic Doppler current profiler (ADCP) is at least as accurate as estimates from empirical formulas. The simultaneous ADCP measurements and tracer studies of Shen et al. (2010) showed that the dispersion coefficient from (2) matched direct measurements from tracer studies well.

Now that velocity fields can be measured in detail over the cross section of a channel, the effects of both transverse and vertical variations of velocity can be included in calculations of the dispersion coefficient, but the question of whether accounting for both is necessary remains to be answered. Kim (2012) developed algorithms to compute both K_T and K_V from ADCP data, though he applied them separately depending on whether vertical mixing and transverse mixing were complete. Fischer et al. (1979, p. 129) argued that because the dispersion coefficient is proportional to the square of the distance over

which tracer is spreading normal to the flow and because the channel aspect ratio H/B usually exceeds 10, vertical variations will contribute 1% or less to the overall dispersion. However, because the dispersion coefficient is also inversely proportional to the mixing coefficient—as in equations (2) and (3), the important parameter is not the aspect ratio H/B but the ratio of mixing times $\tau = (H^2/D_z)/(B^2/D_y)$. Although the aspect ratio is usually large, so is the ratio D_y/D_z . The vertical mixing coefficient is often estimated with $D_z / u_* H = 0.067$ (Fischer et al. 1979, p. 106) where u_* is the shear velocity; then the formula $D_y / u_* H = 0.6$ (Fischer et al. 1979, p. 112) for the transverse mixing coefficient in gently meandering channels gives $D_y/D_z \approx 9$. However, because $D_y / u_* H$ can reach 10 in channels with sharp bends (Rutherford, 1994, p. 113), D_y/D_z can be as large as 150. Therefore, vertical variations in velocity might affect dispersion more than others have assumed.

To estimate the effect, we derive an expression for the longitudinal dispersion coefficient in a channel with simple geometry that accounts for both transverse and vertical variations in velocity. The velocity variations are modeled using functions from work of previous researchers. After developing the model in the next section, data from field observations are used to estimate the time scale ratio τ and quantify the importance of vertical variations of velocity for dispersion.

Methods

The calculation of the dispersion coefficient follows the analyses of Fischer et al. (1979, pp. 82-87) and Young and Jones (1991). If the mixing coefficients are assumed to be

constant and a coordinate $\xi = x - \bar{u}t$ moving with the mean velocity is used, then averaging equation (1) over the cross section and subtracting the result from (1) yields

$$\frac{\partial C'}{\partial t} + u' \frac{\partial \bar{C}}{\partial \xi} + u' \frac{\partial C'}{\partial \xi} - \overline{u' \frac{\partial C'}{\partial \xi}} = D_x \frac{\partial^2 C'}{\partial \xi^2} + D_y \frac{\partial^2 C'}{\partial y^2} + D_z \frac{\partial^2 C'}{\partial z^2} \quad (32)$$

where $C' = C - \bar{C}$ is the concentration deviation and \bar{C} is the concentration averaged over the cross-sectional area. Estimating terms in a way similar to that of Young and Jones (1991) shows that the first term is negligible if the time scale of evolution is much greater than the diffusion time B^2/D_y and that the fifth term is negligible if the width and depth are much smaller than the streamwise length L . The ratio of the third term and the second term is

$$\frac{u' \partial C' / \partial \xi}{u' \partial \bar{C} / \partial \xi} \sim \frac{\bar{u} \Delta C / L}{\bar{u} \bar{C} / L} \quad (33)$$

The parameter ΔC , which is the scaling estimate for the concentration deviation, can be estimated from the solution of Fischer et al. (1979, eq. 4.14),

$$C' = \frac{1}{D_y} \frac{\partial \bar{C}}{\partial x} \int_0^y \int_0^{y_1} u' dy_1 dy + C'(0) \sim \Delta C \sim \frac{\bar{C} \bar{u} B^2}{D_y L} \quad (34)$$

Combining (5) and (6) shows that the third term can be neglected if $(\bar{u}B / D_y)(B / L) \ll 1$, or if the transverse mixing time B^2/D_y is much smaller than the advection time L / \bar{u} ; a similar argument can be used to neglect the fifth term when $(\bar{u}H / D_z)(H / L) \ll 1$. Then the concentration deviation is governed by a Poisson equation

$$D_y \frac{\partial^2 C'}{\partial y^2} + D_z \frac{\partial^2 C'}{\partial z^2} = u' \frac{\partial \bar{C}}{\partial \xi} \quad (35)$$

with no-flux boundary conditions on the banks, bottom, and water surface—that is, $\partial C' / \partial y = 0$ on $y = 0$ and $y = B$ and $\partial C' / \partial z = 0$ on $z = 0$ and $z = H$. The concentration deviation is determined using eigenfunction expansions (Zauderer, 1989, pp. 207-218):

$$C'(y, z) = \sum_{n=0}^{\infty} \sum_{m=0}^{\infty} C_{mn} \phi_{mn}(y, z) = -\frac{\partial \bar{C}}{\partial \xi} \sum_{n=0}^{\infty} \sum_{m=0}^{\infty} \frac{U_{mn}}{\lambda_{mn}} \phi_{mn}(y, z) \quad (36)$$

where m and n are mode numbers, $\lambda_{mn} = D_y(m\pi/B)^2 + D_z(n\pi/H)^2$ are the eigenvalues, $\phi_{mn} = \cos(m\pi y/B)\cos(n\pi z/H)$ are the eigenfunctions, C_{mn} are the coefficients for the expansion of the concentration deviation, and

$$U_{mn} = \frac{\int_0^H \int_0^B u'(y, z) \cos\left(\frac{m\pi y}{B}\right) \cos\left(\frac{n\pi z}{H}\right) dydz}{\int_0^H \int_0^B \cos^2\left(\frac{m\pi y}{B}\right) \cos^2\left(\frac{n\pi z}{H}\right) dydz} \quad (37)$$

Because of the no-flux boundary conditions, the solution in equation (8) is not unique: Equation (8) with any additive constant is still a solution of (7) and the boundary conditions. However, as in the one-dimensional case (Fischer et al. 1979, p. 85), the constant does not affect the mass flux \dot{M} , which is computed by integrating the product of the velocity deviation and concentration deviation over the cross section:

$$\dot{M} = \int_0^H \int_0^B u'(y, z) C'(y, z) dydz \quad (38)$$

If the mass flux is expressed in terms of a dispersion coefficient K as $\dot{M} = -KHB(\partial \bar{C} / \partial \xi)$, then the dimensionless dispersion coefficient $K^* = KD_y / \bar{u}^2 B^2$ is

$$\begin{aligned} K^* = & \frac{2}{\pi^2} \sum_{m=1}^{\infty} \frac{1}{m^2} \left[\int_0^1 \int_0^1 \frac{u'(\eta, \zeta)}{\bar{u}} \cos(m\pi\eta) d\eta d\zeta \right]^2 \\ & + \frac{2\tau}{\pi^2} \sum_{n=1}^{\infty} \frac{1}{n^2} \left[\int_0^1 \int_0^1 \frac{u'(\eta, \zeta)}{\bar{u}} \cos(n\pi\zeta) d\eta d\zeta \right]^2 \\ & + \frac{4}{\pi^2} \sum_{n=1}^{\infty} \sum_{m=1}^{\infty} \frac{1}{m^2 + \tau^{-1}n^2} \left[\int_0^1 \int_0^1 \frac{u'(\eta, \zeta)}{\bar{u}} \cos(m\pi\eta) \cos(n\pi\zeta) d\eta d\zeta \right]^2 \end{aligned} \quad (39)$$

where $\eta = y/B$ and $\zeta = z/H$. The three terms arise from the cases $m = 0$, $n = 0$, and $m, n \neq 0$, respectively. After the velocity profile is specified, the dispersion coefficient can be computed as a function of the time scale ratio τ .

The velocity profile is based on functions that previous researchers have used to describe the transverse and vertical variations of velocity. The velocity, normalized by the cross-sectional average velocity so that results from different profiles can be compared, is taken to be $u/\bar{u} = f(\eta)g(\zeta)$, and examples of model profiles used in the analysis are shown in Fig. 1a and b. The function $f(\eta)$, which describes the transverse variation (Fig. 1a), was proposed by Seo and Baek (2004) to be

$$f(\eta) = \frac{\Gamma(\alpha + \beta)}{\Gamma(\alpha)\Gamma(\beta)} \eta^{\alpha-1} (1-\eta)^{\beta-1} \quad (40)$$

where $\Gamma(\alpha)$ is the gamma function and α and β are parameters controlling the shape of the profile. The profile is uniform when $\alpha = \beta = 1$, and as both values increase, the profile becomes more non-uniform and the range of velocities increases. When α and β are not equal, the profile becomes asymmetric. Typical values of both α and β range from 1 to 4.5 (Fig. 2), as Seo and Baek (2004) showed by fitting (12) to datasets from four rivers studied by Godfrey and Frederick (1970). Profiles with $\alpha = \beta = 1.2$ and $\alpha = \beta = 2$ are considered because most values of both α and β cluster between 1 and 2, and a profile with $\alpha = \beta = 4$ is used to examine the effects of more non-uniform profiles.

The function describing the vertical profile is taken to be either logarithmic or a power law (Fig. 1b). In the former case, $g(\eta) = \ln(\zeta H/z_0)/\ln(e^{-1}H/z_0)$, where z_0 is a roughness length. The profile for $H/z_0 = 10^5$ is shown in Fig. 1b; as H/z_0 increases, the profiles become more uniform, and the change in velocity is concentrated closer to the

boundary. Power-law profiles are described with $g(\eta) = (r+1)\zeta^r$, where r is an exponent; profiles become less uniform as r increases (Fig. 1b). Barenblatt and Chorin (1996) argued that the exponent for flow in a pipe can be computed as $r = 3/(2\ln Re)$, where Re is the Reynolds number based on the mean velocity and pipe diameter. Using this relation to estimate r from the data sets compiled in Rutherford (1994, pp. 194-197), Seo and Cheong (1998), Kashefipour and Falconer (2002), Seo and Baek (2004), and Jackson et al. (2012) gives an approximate range of $0.09 < r < 0.13$.

Ranges of the time scale ratio τ were estimated from field measurements in rivers and empirical expressions for the mixing coefficients D_z and D_y . The data sets from the references cited above were used to obtain values for the channel width, channel depth, mean velocity, and shear velocity u_* . The vertical mixing coefficient was estimated with $D_z = 0.067u_*H$ (Fischer et al. 1979, p. 106), which was derived using assumptions similar to those leading to the logarithmic velocity profile. The transverse mixing coefficient D_y was estimated with several empirical formulas (Table 1). Because the data sets described above do not include sinuosity S_n , which is included in the formula from Jeon et al. (2007), values of $S_n = 1$ and 2 were considered; these values cover the range of sinuosities in Jeon et al. (2007).

Results and Discussion

For the case of a rectangular cross section, the role of transverse and vertical variations on dispersion can be identified. The first term in (11) is the dispersion coefficient resulting from only transverse variations, while the second term is the dispersion coefficient resulting from only vertical variations. The first and second terms can be derived by substituting the eigenfunction expansion for the velocity deviation in (2) and (3),

respectively. The third term involves effects of both transverse and vertical variations. Because K^* is made dimensionless with $\bar{u}^2 B^2 / D_y$ —the scaling expected in a case when only transverse variations are important, the time scale ratio τ appears in only the second and third terms. The analysis shows that once the velocity profile is specified, the dimensionless dispersion coefficient depends only on τ . The appearance of the time scale ratio as the key parameter in this more detailed analysis is consistent with the simple scaling used in the introduction.

The normalized dispersion coefficient varies between the limits for cases when either transverse variations or vertical variations control the spreading (Fig. 3). For small τ , K^* approaches a constant because only transverse variations control the dispersion—that is, the first term in (11) dominates. As noted above, equation (2) provides a good estimate of the dispersion coefficient if the depth-averaged velocity is used. For large τ , K^* increases linearly with τ , as seen from the second term in equation (11) or the argument that since $K \propto \bar{u}^2 H^2 / D_z$ when vertical variations control the dispersion, then $K^* \propto \tau$. For intermediate values of τ , K^* varies smoothly between the two limits.

Profiles that are more uniform have smaller dispersion coefficients. For example, in the case of symmetric profiles ($\alpha = \beta$), smaller values of the shape parameters lead to smaller values of K^* (Fig. 3). This result holds in the one-dimensional case as well. It also applies to vertical variations, but the profiles considered here are so similar that differences in the dispersion coefficient are small. Effects of asymmetry (e.g., $\alpha \neq \beta$) can also be assessed in the model, but the results do not differ much from results from the symmetric cases.

The model allows the relative contributions of transverse and vertical variations to be assessed (Fig. 4). Small values of α and β are used in Fig. 4 because vertical variations are more important when transverse variations are small. The choice $\alpha = \beta = 1.2$ is near the low end of the range of the shape parameters in Fig. 2. Vertical variations contribute 1% of K^* at $\tau \approx 4 \times 10^{-3}$, 10% at $\tau \approx 0.04$, and an amount equal to the contribution from transverse variations at $\tau \approx 0.4$. The term involving both transverse and vertical variations—the third term in equation (11)—accounts for less than 1% of K^* when $\alpha = \beta = 1.2$; this result also holds for values of the shape parameters near the high end of the range in Fig. 2.

Vertical variations in velocity are likely to be unimportant for determining dispersion in the far field of most waterways (Fig. 5). For the rivers in the data set considered, in which τ ranges from about 10^{-4} to 10^{-1} , vertical variations contribute less than 25% even for more uniform profiles such as those with $\alpha = \beta = 1.2$, as shown in Fig. 5. When the shape parameters are larger, vertical variations are less important. The larger aspect ratio H/B in canals leads to larger values of τ , but still the contribution from vertical variations in all but one case is likely to be less than 25% of the total. This conclusion holds for each of the different estimates of D_y used in Fig. 5.

These results suggest that vertical variations can be neglected. Uncertainty of 25% (say) caused by neglecting vertical variations likely falls within the range of uncertainty of empirical formulas; for example, about two-thirds of the estimates from the formula of Kashefipour and Falconer (2002) differ by 25% or more from the measured values of the dispersion coefficient. Also, shear dispersion is only one of several processes leading to spreading of contaminant clouds; other processes include interaction with recirculation

zones, variations in channel geometry, and flow around islands. Furthermore, vertical variations should be included only if the approximations used in simplifying equation (4) are consistent. For example, if $\tau = 0.1$, then B/L and $(\bar{u}B / D_y)(B / L)$ must be smaller than 0.1 or else the effects of the neglected terms in (4) should be considered.

While this analysis confirms the usual practice of considering only transverse variations of velocity in dispersion estimates, it illustrates that the time scale ratio τ —and not just the aspect ratio H/B —is the key parameter to check. The aspect ratio in the data set used in creating Fig. 5 is small; the largest value is 0.45 for Yuma Mesa Canal. However, D_y/D_z is usually greater than 1. For example, the empirical formulas from Fischer et al. (1979, pp. 106-112) give $D_y/D_z \approx 9$, and values in the data set for Fig. 5 range from 0.1 to 88. The ratio of mixing coefficients was less than 1 only for some estimates with the Bansal (1971) formula for D_y . In principle, an aspect ratio as small as 0.1 could still give $\tau \approx 1$. However, in the data set of Fig. 5 all cases but one had τ less than about 0.1.

If a case occurred in which $\tau \approx 1$, vertical variations of velocity could be included in computing the dispersion coefficient. For rectangular channels at least, because the third term in (11) contributes less than about 1% to K^* , the dispersion coefficient can be computed by simply adding K_T and K_V in Eqs. (2) and (3), respectively. Although this simple geometry is rarely found in waterways, it might be a suitable approximation for canals, which tend to have larger values of H/B and τ (Fig. 5). In waterways with more complex geometry, the Poisson equation (7) would have to be solved again. Numerical solution would have to handle the fact that the concentration deviation is specified only to an additive constant. Another approach would be to use conformal mapping to transform the channel cross section—which can be expressed as a polygon—to a simpler domain

(e.g., the upper half-plane), solve the Poisson equation there, and transform back to the original geometry.

Conclusion

To determine the importance of vertical variations in velocity for dispersion, we extended the analysis of shear dispersion to two dimensions. While in one dimension, solving for the concentration deviation requires integrating, in two dimensions it requires solving a Poisson equation. The analysis supports scaling arguments based on formulas for the dispersion coefficient when either transverse or vertical variations dominate and shows that the contribution of vertical variations to dispersion depends not on the ratio of the width B and depth H of the channel but on the ratio of mixing times, $\tau = (H^2/D_z)/(B^2/D_y)$. Three terms compose the dispersion coefficient for a rectangular channel: one that depends on transverse variations only, one that depends on vertical variations only, and one that depends on both. The first does not depend on τ , while the other two do. The terms were compared by using analytical functions for velocity profiles and a set of data on rivers and canals compiled from several sources. Although the ratio D_y/D_z can reach $O(10^2)$, the time scale ratio was smaller than 0.1 in all but one case. Therefore, the term depending on both transverse and vertical variations is likely to be negligible, while the term depending on vertical variations only is likely to be important rarely. The analysis supports the usual practice of considering only transverse variations in computing the dispersion coefficient, and it clarifies the conditions for assessing the importance of vertical variations and outlines an approach for including them in calculations of dispersion.

Notation

A	=	area of the cross section;
B	=	top width of the channel;
$b(z)$	=	width at vertical position z ;
C	=	concentration;
\bar{C}	=	concentration averaged over the cross section;
C'	=	deviation from the average concentration \bar{C} ;
C_{mn}	=	coefficients in the eigenfunction expansion of C' ;
ΔC	=	scaling estimate for the concentration deviation;
D_x	=	streamwise mixing coefficient;
D_y	=	transverse mixing coefficient;
D_z	=	vertical mixing coefficient;
$f(\eta)$	=	function describing the transverse variation of velocity;
$g(\zeta)$	=	function describing the vertical variation of velocity;
H	=	maximum depth of the channel;
$h(y)$	=	depth as a function of the transverse position y ;
K	=	longitudinal dispersion coefficient;
K_T	=	longitudinal dispersion coefficient assuming transverse variations control spreading;
K_V	=	longitudinal dispersion coefficient assuming vertical variations control spreading;
K^*	=	$KD_y / \bar{u}^2 B^2$;
L	=	streamwise length;

\dot{M}	=	mass flux;
m	=	eigenfunction mode number for the transverse direction;
n	=	eigenfunction mode number for the vertical direction;
Re	=	Reynolds number;
r	=	exponent in power-law function for vertical variation of velocity;
S_n	=	sinuosity;
t	=	time;
U_{mn}	=	coefficients in the eigenfunction expansion of u' ;
\hat{u}	=	streamwise velocity;
\bar{u}	=	velocity averaged over the cross section;
u'	=	deviation from the average velocity \bar{u} ;
\hat{u}	=	deviation—averaged over the depth—from the mean velocity \bar{u} ;
\tilde{u}	=	deviation—averaged over the width—from the mean velocity \bar{u} ;
u_*	=	shear velocity;
x	=	streamwise coordinate;
y	=	transverse coordinate;
z	=	vertical coordinate;
z_0	=	roughness length;
α	=	shape parameter for the function in equation (12);
β	=	shape parameter for the function in equation (12);
$\Gamma(\alpha)$	=	gamma function;
ζ	=	z/H , dimensionless vertical coordinate;
η	=	y/B , dimensionless transverse coordinate;

λ_{mn} = eigenvalue;

ξ = $x - \bar{u}t$, coordinate moving with the mean velocity;

τ = $(H/B)^2(D_y/D_z)$;

ϕ_{mn} = eigenfunction;

References

- Bansal, M. K. (1971). "Dispersion in natural streams." *J. Hydraul. Div. ASCE*, 97(11), 1867-1886.
- Barenblatt, G. I., and Chorin, A. J. (1996). "Small viscosity asymptotics for the inertial range of local structure and for the wall region of wall-bounded turbulent shear flow." *Proc. Nat. Acad. Sci. USA*, 93(13), 6749-6752.
- Carr, M. L., and Rehmann, C. R. (2007). "Measuring the dispersion coefficient with acoustic Doppler current profilers." *J. Hydraul. Eng.*, 133(8), 977-982.
- Deng, Z. Q., Singh, V. P., and Bengtsson, L. (2001). "Longitudinal dispersion coefficient in straight rivers." *J. Hydraul. Eng.*, 127(11), 919-927.
- Elder, J. W. (1959). "The dispersion of marked fluid in turbulent shear flow." *J. Fluid Mech.*, 5(4), 544-560.
- Fischer, H. B. (1967). "The mechanics of dispersion in natural streams." *J. Hydraul. Div. ASCE*, 93(HY 6), 187-216.
- Fischer, H. B., List, E. J., Koh, R. C. Y., Imberger, J., and Brooks, N. H. (1979). *Mixing in Inland and Coastal Waters*, Academic Press, New York.
- Godfrey, R. G., and Frederick, B. J. (1970). "Stream dispersion at selected sites." Professional Paper No. 433-K, U.S. Geological Survey, Washington, D.C.
- Jackson, P. R., Johnson, K. K., and Duncker, J. J. (2012). "Comparison of index velocity measurements made with a horizontal acoustic Doppler current profiler and a three-path acoustic velocity meter for computation of discharge in the Chicago Sanitary and Ship Canal near Lemont, Illinois." U.S. Geological Survey Scientific Investigations Report 2011-5205. U.S. Geological Survey, Reston, VA.

- Jeon, T. M., Baek, K. O., and Seo, I. W. (2007). "Development of an empirical equation for the transverse dispersion coefficient in natural streams." *Environ. Fluid Mech.*, 7(4), 317-329.
- Kashefipour, S. M., and Falconer, R. A. (2002). "Longitudinal dispersion coefficients in natural channels." *Water Res.*, 36(6), 1596-1608.
- Kim, D. (2012). "Assessment of longitudinal dispersion coefficients using acoustic Doppler current profilers in large river." *J. Hydro-Environment Res.*, 6(1), 29-39.
- Rutherford, J. C. (1994). *River Mixing*, Wiley, Chichester, UK.
- Seo, I. W., and Baek, K. O. (2004). "Estimation of the longitudinal dispersion coefficient using the velocity profile in natural streams." *J. Hydraul. Eng.*, 130(3), 227-236.
- Seo, I. W., and Cheong, T. S. (1998). "Predicting longitudinal dispersion coefficient in natural streams." *J. Hydraul. Eng.*, 124(1), 25-32.
- Shen, C., Niu, J., Anderson, E. J., and Phanikumar, M. S. (2010). "Estimating longitudinal dispersion in rivers using acoustic Doppler current profilers." *Adv. Water Resour.*, 33(6), 615-623.
- Taylor, G. I. (1953). "Dispersion of soluble matter in solvent flowing slowly through a tube." *Proc. R. Soc. London A*, 219, 186-203.
- Young, W. R., and Jones, S. (1991). "Shear dispersion." *Phys. Fluids A*, 3(5), 1087-1101.
- Zauderer, E. (1989). *Partial Differential Equations of Applied Mathematics*, Wiley, New York.

Table 7 Empirical formulas used to estimate the transverse mixing coefficient D_y .

Source	Formula
Fischer et al. (1979)—straight	$\frac{D_y}{u_* H} = 0.15$
Fischer et al. (1979)—gently meandering	$\frac{D_y}{u_* H} = 0.6$
Bansal (1971)	$\frac{D_y}{u_* H} = 0.002 \left(\frac{B}{H} \right)^{1.5}$
Deng et al. (2001)	$\frac{D_y}{u_* H} = 0.145 + \frac{1}{3,520} \left(\frac{\bar{u}}{u_*} \right) \left(\frac{B}{H} \right)^{1.38}$
Jeon et al. (2007)	$\frac{D_y}{u_* H} = 0.03 \left(\frac{\bar{u}}{u_*} \right)^{0.46} \left(\frac{B}{H} \right)^{0.30} S_n^{0.73}$

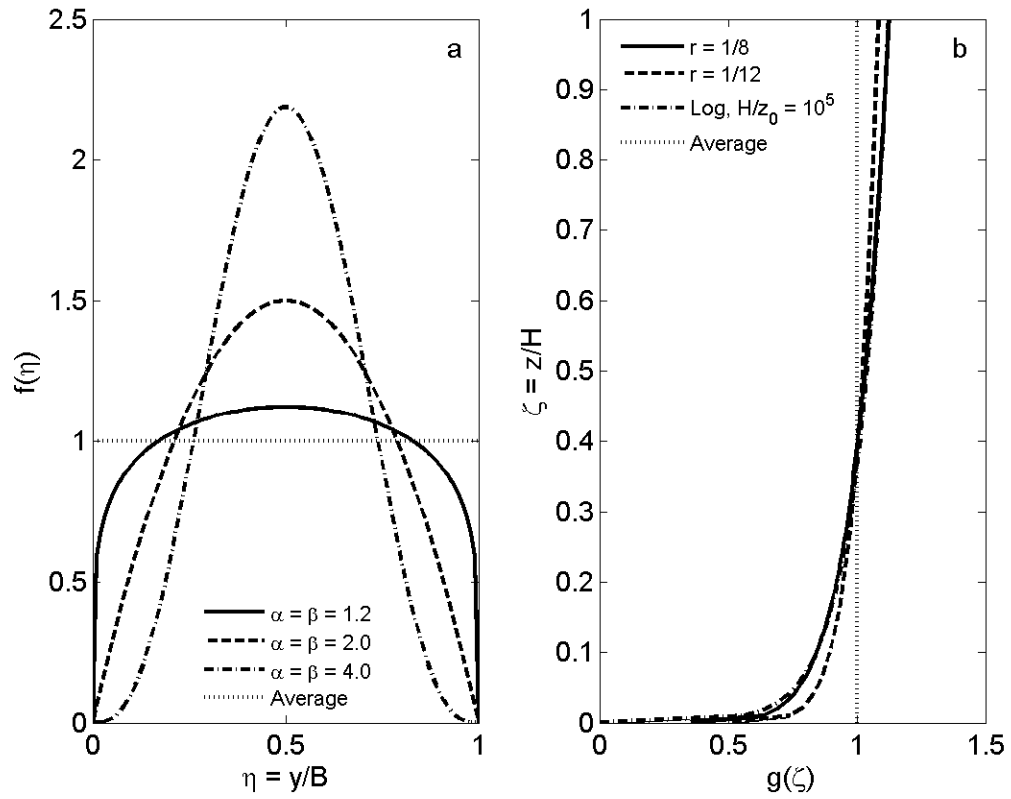


Fig. 23. Examples of model velocity profiles: (a) transverse variation, (b) vertical variation.

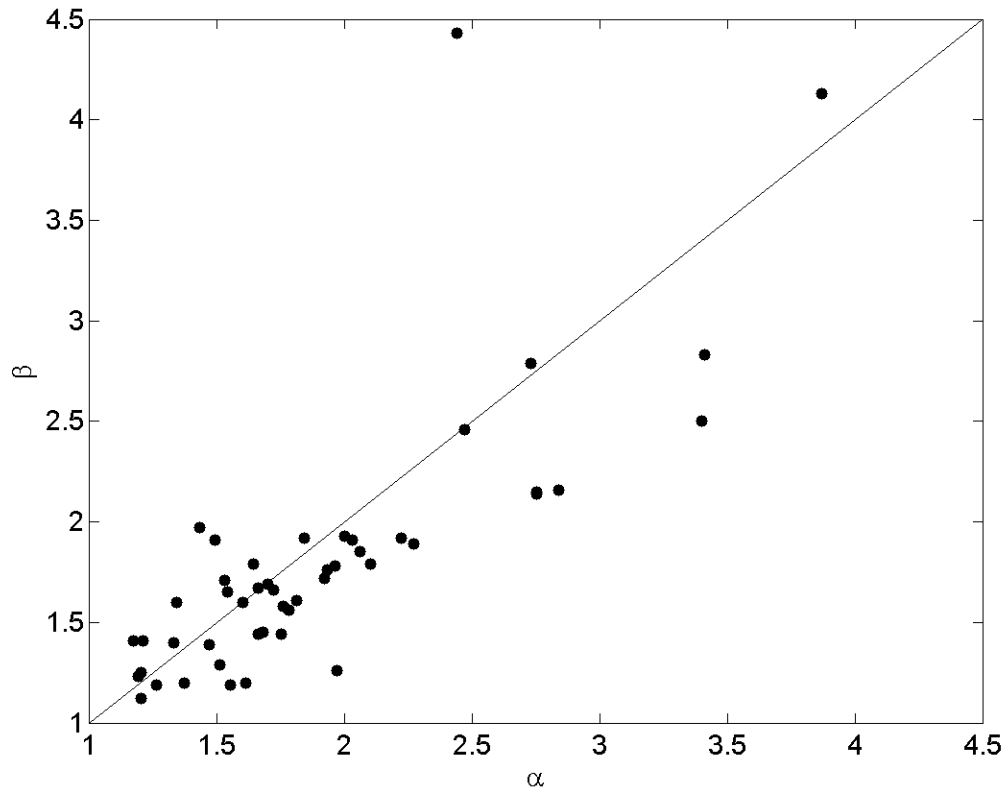


Fig. 24. Shape parameters α and β computed by Seo and Baek (2004) from field measurements of Godfrey and Frederick (1970).

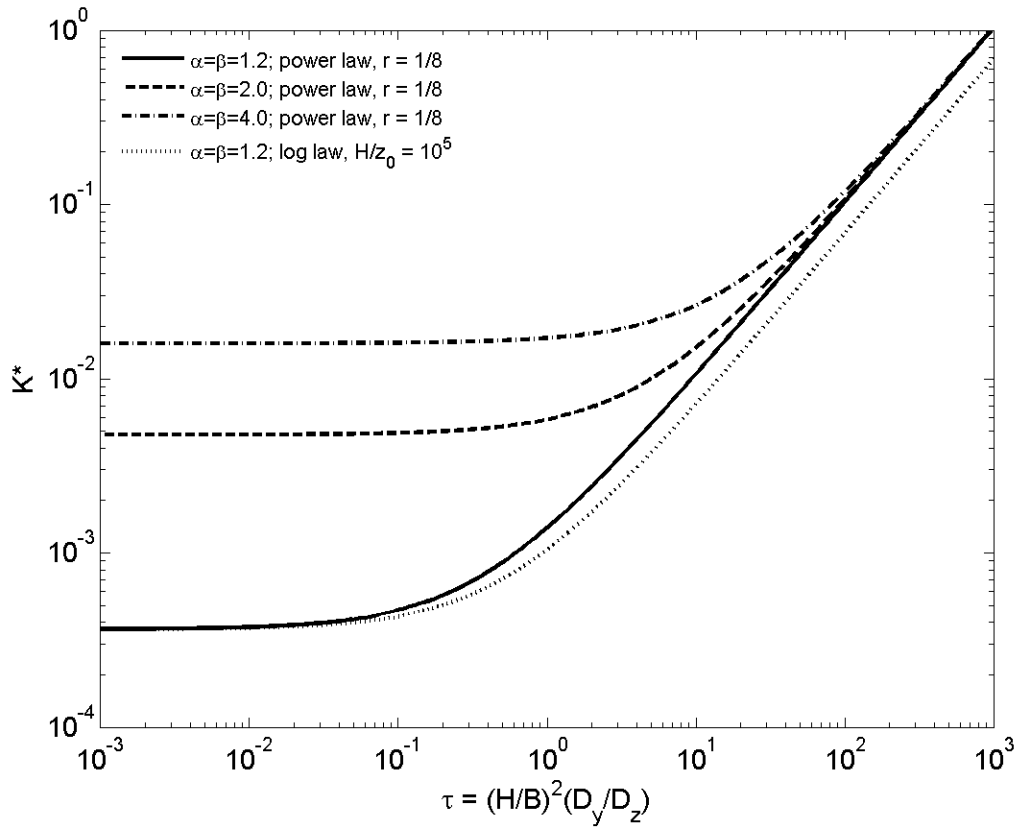


Fig. 25. K^* as a function of the time scale ratio τ for different profile shapes.

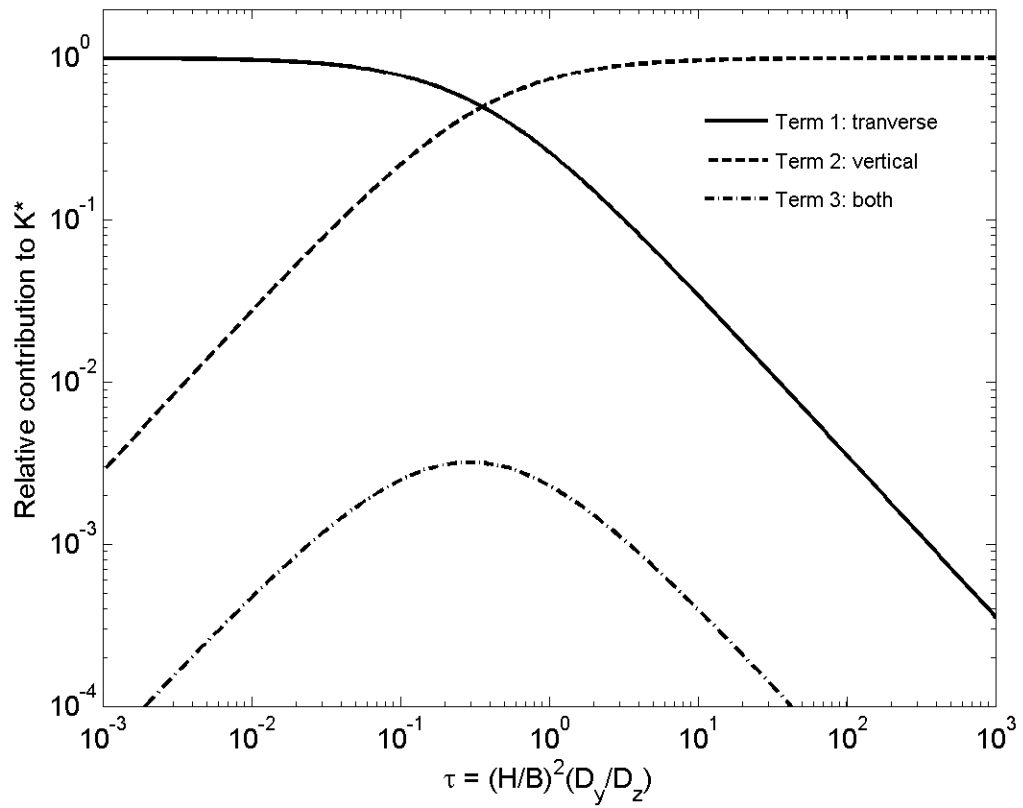


Fig. 26. Fraction of K^* contributed by the three terms in equation (11). The velocity profile has $\alpha = \beta = 1.2$ and $r = 1/8$.

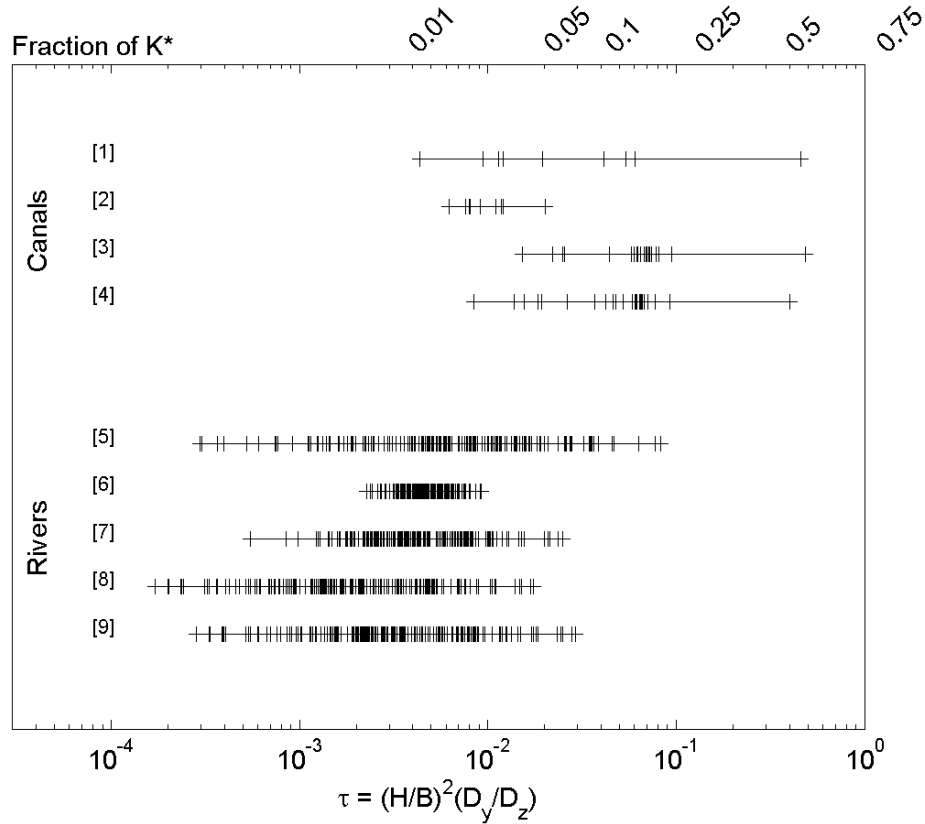


Fig. 27. Ranges of the time scale ratio τ computed from the data sets compiled by Rutherford (1994), Seo and Cheong (1998), Kashefipour and Falconer (2002), Seo and Baek (2004), and Jackson et al. (2012). Formulas for D_y (Table 1) were [1] Fischer et al. (1979), straight channels, [2] and [6] Bansal (1971), [3] and [7] Deng et al. (2001), [4] and [8], Jeon et al. (2007), $S_n = 1.0$; [5] Fischer et al. (1979), gently meandering channels; [9] Jeon et al. (2007), $S_n = 2.0$. The scale on the top axis shows the fraction of K^* contributed by the second term in (11) for profiles with $\alpha = \beta = 1.2$ and power-law variation with $r = 1/8$.

APPENDIX B: MATLAB SCRIPTS USED IN READING AND PROCESSING ADCP AND ADV DATA

ADCP Utilities

ADCP_read_2

```
function [V,ens,bindepth] = ADCP_read_2(filename,pathname)

% ADCP_read_2  Read beam velocities from a StreamPro file
%
%   Chris Rehmann, 7-18-15

% Set constants

nbeam = 4;           % Number of beam
nfield = nbeam + 1; % Number of data fields (bin depths and beam
velocities)
maxens = 10000;     % Maximum number of ensembles

% Open the file

fid = fopen([pathname filename]);

% Read line by line

count = 0;
ens = NaN*ones(maxens,1);

while ~feof(fid)
    str = fgetl(fid);
    count = count + 1;
    dlmpos = [findstr(str,'$$') length(str)+1];
    ens(count) = uint32(str2num(str(1:dlmpos(1)-1)));
    if count == 1
        C = textscan(str(dlmpos(1)+2:dlmpos(2)-
1),'%f','Delimiter',' ');
        bindepth = C{1};
        nbin = length(bindepth);
        V = NaN*ones(maxens,nbin,nbeam);
    end
    for ifield = 2:nfield
        ibeam = ifield-1;
        substr = str(dlmpos(ifield)+2:dlmpos(ifield+1)-1);
        C = textscan(substr,'%f','Delimiter',' ');
        V(count,1:nbin,ibeam) = C{1};
    end
end

% Close the file

fclose(fid);
```

```
% Strip the NaNs

ens = ens(1:count);
V   = V(1:count, :, :);

% Replace the bad velocities with NaNs

V(V == -32768) = NaN;
```

ADCP_process_f

```

function
[xypa,xzpa,yzpa,uav14,uav23,vav13,vav24,wav12,wav34,bindepth,xxpa,yya,
zzpa] = ADCP_process_f(filenameADCP,pathnameADCP)

% ADCP_process
%
% Process Reynolds stresses from StreamPro ADCP measurements. Beams are
% oriented in the Janus configuration and pointed 45 degrees off the
% direction of flow. Units of input file are in metric and meters.
Units of
% output are in centimeters to match outputs of ADV.

% Open the StreamPro transect file

% [filename,pathname] = uigetfile('.txt','Select the StreamPro
file');

% Load and extract beam velocity data

[V,ens,bindepth] = ADCP_read_2(filenameADCP,pathnameADCP);
[wack,a,mole] = size(V);

bindepth = bindepth.*100;

disp(['Processing file ' filenameADCP])

% Set up angles in radians for MATLAB

alf = (45/180)*pi(); % The beams are oriented 45* from the x & y
axis
gam = (20/180)*pi(); % The beams look downward at 20* from
vertical

% Set up empty matrices

xypa = NaN.*ones(size(a));
xzpa = NaN.*ones(size(a));
yzpa = NaN.*ones(size(a));
uav14 = NaN.*ones(size(a));
uav23 = NaN.*ones(size(a));
vav13 = NaN.*ones(size(a));
vav24 = NaN.*ones(size(a));
wav12 = NaN.*ones(size(a));
wav34 = NaN.*ones(size(a));

% Set up looping to calculate for each depth

for n = 1:a

% Extract individual beams

```

```

V1 = V(:,n,1)*100;
V2 = V(:,n,2)*100;
V3 = V(:,n,3)*100;
V4 = V(:,n,4)*100;

% Compute beam averages ignoring NaNs

V1av = nanmean(V1);
V2av = nanmean(V2);
V3av = nanmean(V3);
V4av = nanmean(V4);

% Calculate the beam fluctuations

V1f = V1-V1av;
V2f = V2-V2av;
V3f = V3-V3av;
V4f = V4-V4av;

% Multiply the different components you need

V11f = V1f.*V1f;
V22f = V2f.*V2f;
V33f = V3f.*V3f;
V44f = V4f.*V4f;
V13f = V1f.*V3f;
V24f = V2f.*V4f;
V23f = V2f.*V3f;
V14f = V1f.*V4f;
V12f = V1f.*V2f;
V34f = V3f.*V4f;

% Compute averages of the multiplied components

V11a = nanmean(V11f);
V22a = nanmean(V22f);
V33a = nanmean(V33f);
V44a = nanmean(V44f);
V13a = nanmean(V13f);
V24a = nanmean(V24f);
V23a = nanmean(V23f);
V14a = nanmean(V14f);
V12a = nanmean(V12f);
V34a = nanmean(V34f);

% Kick out stress averages

xya(n) = (V33a-V11a+V44a-
V22a)/(8*cos(alf)*cos(alf)*sin(gam)*sin(gam));
xzpa(n) = (V22a-V11a+V44a-V33a)/(8*cos(alf)*sin(gam)*cos(gam));
yzpa(n) = -(V22a-V11a+V33a-
V44a)/(8*sin(alf)*sin(gam)*cos(gam));
%      xzpa2(n) = (V24a-V13a)/(4*cos(gam)*cos(alf)*sin(gam));
%      yzpa2(n) = (V23a-V14a)/(4*cos(gam)*cos(alf)*sin(gam));

```

```

%      xypa2(n) = (V12a-
V34a)/(4*sin(gam)*sin(gam)*cos(alf)*sin(alf));

      xxpa(n) = nanmean((V1f-V4f+V3f-V2f).*(V1f-V4f+V3f-
V2f)/(16*cos(alf)*sin(gam)*cos(alf)*sin(gam)));
      yypa(n) = nanmean((V1f-V3f+V4f-V2f).*(V1f-V3f+V4f-
V2f)/(16*cos(alf)*sin(gam)*cos(alf)*sin(gam)));
      zzpa(n) =
nanmean((V1f+V2f+V3f+V4f).*(V1f+V2f+V3f+V4f)/(16*cos(gam)*cos(gam)));
%      xxpa2(n) = (1/(2*sin(alf)*sin(alf)*sin(gam)*sin(gam)))*(V11a-
V14a+0.5*(V12a+V24a-V13a-V34a));
%      yypa2(n) = (1/(2*cos(alf)*cos(alf)*sin(gam)*sin(gam)))*(V22a-
V24a+0.5*(V12a+V14a-V23a-V34a));
%      zzpa2(n) =
(1/(2*cos(gam)*cos(gam)))*(V44a+V34a+0.5*(V13a+V23a-V24a-V14a));

% Kick out average velocity components

      uav14(n) = (V1av-V4av)/(2*cos(alf)*sin(gam));
      uav23(n) = (V3av-V2av)/(2*cos(alf)*sin(gam));
      vav13(n) = (V1av-V3av)/(2*cos(alf)*sin(gam));
      vav24(n) = (V4av-V2av)/(2*cos(alf)*sin(gam));
      wav12(n) = (V1av+V2av)/(2*cos(gam));
      wav34(n) = (V3av+V4av)/(2*cos(gam));

```

end

ADV Utilities

ADV_read_condensed

```

function [Vx,Vy,Vz,Vxgood,Vygood,Vzgood,t,tg] =
ADV_read_condensed(filenameADV,pathnameADV)

% Function for reading in data
% Based on ADV_ANALYZE_SINGLE by Chris Rehmann. Reads in ADV file.
Computes
% statistics for velocities. Returns the good points as a new matrix.
%
% ADV_ANALYZE_SINGLE Compute statistics of velocity measured with an
ADV
% Chris Rehmann, 1-12-10

% Set the path

    codedir = pwd;
    addpath(codedir)

% Set constants

    delimstr = ' '; % Delimiter for the ADV files
    startrow = 10; % Starting row of data in ADV files
    startcol = 0; % Starting column of data in ADV files
    mincor = 70; % Minimum correlation
    minSNR = 5; % Minimum SNR
    alpha = 0.01; % Convergence criterion for averaging
    nbins = 40; % Number of bins for histogram

% Process

% clc; disp(['Filename Vx mean Vy mean Vz mean % good %
spike Tavgx (s) Tavgy (s) Tavgz (s)'])

    data = dlmread([pathnameADV
filenameADV],delimstr,startrow,startcol); % Get the data
    ntotal = % Find
size(data,1); % Find
the number of points

    Vx = %
data(:,4); %
Get velocities
    Vy = data(:,5);
    Vz = data(:,6);
    t = data(:,1);

    cor0 = data(:,7); SNR0 =
data(:,10); % Get correlation and SNR
    cor1 = data(:,8); SNR1 = data(:,11);

```

```

cor2 = data(:,9);          SNR2 = data(:,12);

spike_indx = find(cor0 ==
0);                          % Spikes have blank
data, or zeros
nspikes =
length(spike_indx) ;          % Number
of spikes
good_indx = find(cor0 >= mincor & cor1 >= mincor & cor2 >= mincor
& ...
SNR0 >= minSNR & SNR1 >= minSNR & SNR2 >= minSNR);
ngood =
length(good_indx);          % Number
of good points

Vxgood =
data(good_indx,4);          %
Extract velocity components
Vygood = data(good_indx,5);
Vzgood = data(good_indx,6);

tg = data(good_indx,1);
Tavgx = avgtime(t,Vx,alpha);
Tavgy = avgtime(t,Vy,alpha);
Tavgz = avgtime(t,Vz,alpha);

%      Column      Variable
%      1           Time (seconds)
%      2           Position
%      3           Flag
%      4           x-velocity
%      5           y-velocity
%      6           z-velocity
%      7           Correlation 0
%      8           Correlation 1
%      9           Correlation 2
%      10          SNR 0
%      11          SNR 1
%      12          SNR 2
%      13          Amplitude 0
%      14          Amplitude 1
%      15          Amplitude 2
%      16          Average correlation
%      17          Average SNR
%      18          Average amplitude

```

ADV_process_f

```

function [xyadv, xzadv, yzadv, ubar, vbar, wbar, z, xxadv, yyadv,
zzadv] = ADV_process_f(depthfileADV,pathnameADV)

% Processing all the depths of data
% The depths represented are the ADCP corresponding value, or depth
% from the surface. Current set to input good data. Can change to be
all
% data.

[Z,fnames,~] = xlsread([pathnameADV
depthfileADV], 'ADV_Depths', 'A10:E500');
dirstruct = dir(pathnameADV);

vert = Z(:,1);
hori = Z(:,4);

count = 0;
for i = 1:length(dirstruct)
    filenameADV = dirstruct(i).name;
    if length(filenameADV) >= 3
        if strcmp(filenameADV(end-2:end),'.Vf')
            indx = find(strcmp(fnames,filenameADV));
            if ~isempty(indx)
                disp(['Processing file ' filenameADV])
                count = count + 1;
                [Vx,Vy,Vz,Vxg,Vyg,Vzg,t,tg] =
ADV_read_condensed(filenameADV,pathnameADV);
                Vxfluc = Vxg-mean(Vxg);
                Vyfluc = Vyg-mean(Vyg);
                Vzfluc = Vzg-mean(Vzg);
                Vxyf = Vxfluc.*Vyfluc;
                Vxzf = Vxfluc.*Vzfluc;
                Vyzf = Vyfluc.*Vzfluc;
                xyn = -1*mean(Vxyf);
                xzn = -1*mean(Vxzf);
                yzn = -1*mean(Vyzf);
                xxn = mean(Vxfluc.*Vxfluc);
                yyn = mean(Vyfluc.*Vyfluc);
                zzn = mean(Vzfluc.*Vzfluc);
                xyadv(count) = xyn;
                xzadv(count) = xzn;
                yzadv(count) = yzn;
                xxadv(count) = xxn;
                yyadv(count) = yyn;
                zzadv(count) = zzn;
                ubar(count) = mean(Vxg);
                vbar(count) = mean(Vyg);
                wbar(count) = mean(Vzg);
                z(count) = vert(indx);
            end
        end
    end
end
end

```


REFERENCES

- Bansal, M. K. (1971) Dispersion in natural streams. *Journal of the Hydraulics Division*, 97, 1867-1886.
- Bogle, G. V. (1997) Stream velocity profiles and longitudinal dispersion. *Journal of Hydraulic Engineering*, 123, 816-820.
- Boxall, J. B. & I. Guymer (2003) Analysis and prediction of transverse mixing coefficients in natural channels. *Journal of Hydraulic Engineering*, 129, 129-139.
- Carr, M. L. & C. R. Rehmann (2007) Measuring the dispersion coefficient with acoustic Doppler current profilers. *Journal of Hydraulic Engineering*, 133, 977-982.
- Deng, Z. Q., V. P. Singh, & L. Bengtsson (2001) Longitudinal dispersion coefficient in straight rivers. *Journal of Hydraulic Engineering*, 127, 919-927.
- Fischer, H. B. (1969) The effect of bends on dispersion coefficients in streams. *Water Resources Research*, 10, 496-506.
- Fischer, H. B., E. J. List, R. C. Y. Koh, J. Imberger & N. H. Brooks (1979) *Mixing in inland and coastal waters*. New York: Academic Press, Inc.
- Fischer, H. B., T. Hanamura (1975) The effect of roughness strips on transverse mixing in hydraulic models. *Water Resources Research*, 11, 362-364
- Gargett, A. E. (1994) Observing turbulence with a modified acoustic Doppler current profiler. *American Meteorological Society*, 11, 1592-1610.

- Goring, D. G. and V. I. Nikora (2002) Despiking acoustic Doppler velocimeter data. *Journal of Hydraulic Engineering*, 128, 117-126.
- Iwasa, Y. and S. Aya (1991) Predicting longitudinal dispersion coefficient in open channel flows. *Proceedings of International Symposium on Environmental Hydraulics*, Hong Kong, 505-510.
- Jeon, T. K., K. O. Baek & I. W. Seo (2007) Development of an empirical equation for the transverse dispersion coefficient in natural streams. *Environmental Fluid Mechanics*, 7, 317-329.
- Joung, Y. and S. Choi (2010) Direct numerical simulation of low Reynolds number flows in an open-channel with sidewalls. *International Journal for Numerical Methods in Fluids*, 62, 854-874.
- Kim, D. (2012) Assessment of longitudinal dispersion coefficients using Acoustic Doppler Current Profilers in large river. *Journal of Hydro-environment Research*, 6, 29-39.
- Koussis, A. D. & J. Rodriguez-Mirasol (1998) Hydraulic estimation of dispersion coefficient for streams. *Journal of Hydraulic Engineering*, 124, 317-320.
- Liu, H. (1977) Predicting dispersion coefficient of streams. *Journal of the Environmental Engineering Division*, 103, 59-69.
- McQuivey, R. S. and T. N. Keefer (1974) Simple method for predicting dispersion in streams. *Journal of the Environmental Engineering Division*, 102, 997-1011

- Nezu, I & H. Nakagawa (1993) *Turbulence in Open Channel Flows*. Rotterdam, Netherlands: A. A. Balkema.
- Nordin, C. F., and G. V. Sabol (1974) Empirical data on longitudinal dispersion in rivers. *U.S. Geological Survey, Water-Resources Investigations*, 332, 20-74.
- Nystrom, E. A., C. R. Rehmann, K. A. Oberg (2007) Evaluation of mean velocity and turbulence measurements with ADCPs. *Journal of Hydraulic Engineering*, 133, 1310-1318.
- Rutherford, J. C. (1994) *River Mixing*. Chichester, UK: John Wiley and Sons Ltd.
- Sayre, W. W. (1979) Shore-attached thermal plumes in rivers. *Journal of the Hydraulics Division*, 104, 709-723.
- Schwab, L. E. & C. R. Rehmann (2015) Importance of vertical variations of velocity for shear dispersion in rivers. *Journal of Hydraulic Engineering*, 141.
- Seo, I. W. & T. S. Cheong (1998) Predicting longitudinal dispersion coefficient in natural streams. *Journal of Hydraulic Engineering*, 124, 25-32.
- Shen, C., J. Niu, E. J. Anderson & M. S. Phanikumar (2010) Estimating longitudinal dispersion in rivers using Acoustic Doppler Current Profilers. *Advances in Water Resources*, 33, 615-623.
- Simpson, M. R., 2001. Discharge Measurements Using a Broad-Band Acoustic Doppler Current Profiler. United States Geological Survey, Open-File Report 01-1.

- Stacey, M. T., S. G. Monismith, J. R. Burau (1999) Measurements of Reynolds stress profiles in unstratified tidal flow. *Journal of Geophysical Research*, 104, 10,933-10,949.
- Teledyne RD Instruments (2011) Acoustic Doppler current profiler principles of operation a practical primer. <http://www.rdinstruments.com>.
- Teledyne RD Instruments (2013) Rio Grande datasheet. <http://www.rdinstruments.com>.
- Teledyne RD Instruments (2015) StreamPro ADCP guide.
<http://www.rdinstruments.com>.
- Teledyne RD Instruments (2016) WinRiverII software user's guide.
<http://www.rdinstruments.com>.
- Tennekes, H. & J. L. Lumley (1989) *A First Course in Turbulence*. Cambridge, Massachusetts: The MIT Press.
- Voulgaris, G., & J. H. Trowbridge (1998) Evaluation of the Acoustic Doppler Velocimeter (ADV) for Turbulence Measurements. *Journal of Atmospheric and Oceanic Technology*, 15, 272-289.
- Yotsukura, N. & W. W. Sayre (1976) Transverse mixing in natural channels. *Water Resources Research*, 12, 695-704.
- Wahl, T. L. (2000) Analyzing ADV data using WinADV. *Joint Conference on Water Resources Engineering and Water Resources Planning and Management*, American Society of Civil Engineers.

Zhang, W. & D. Z. Zhu (2011) Transverse mixing in an unregulated northern river.

Journal of Hydraulic Engineering, 137, 1426-1440.